Chemical Geology 609 (2022) 121039

Contents lists available at ScienceDirect

Chemical Geology

journal homepage: www.elsevier.com/locate/chemgeo

Invited review article

A global review of Hf-Nd isotopes: New perspectives on the chicken-and-egg problem of ancient mantle signatures

Romain Tilhac[a,*], Graham C. Begg[b,c], Suzanne Y. O'Reilly[b], William L. Griffin[b]

[a] Instituto Andaluz de Ciencias de la Tierra (IACT), Consejo Superior de Investigaciones Científicas (CSIC) – Universidad de Granada, 18100 Armilla, Granada, Spain
[b] ARC Centre of Excellence for Core to Crust Fluid Systems (CCFS) and GEMOC, Macquarie University, Sydney, NSW 2109, Australia
[c] Minerals Targeting International, Perth, WA 6005, Australia

ARTICLE INFO

Editor: Catherine Chauvel

Keywords:
Radiogenic isotopes
Sm-Nd and Lu-Hf systems
Isotopic decoupling
Oceanic magmatism
Residual Lithosphere (ReLish)
Mantle heterogeneities
Sub-continental lithospheric mantle (SCLM)
Arc-root delamination
Pyroxenite recycling

ABSTRACT

We present the first global review on the Sm-Nd and Lu-Hf isotope systematics of the mantle; it includes all published data on peridotites and pyroxenites from all tectonic settings (>1100 combined Hf-Nd analyses), as well as previous compilations for oceanic basalts and material such as oceanic and continental sediments. We first provide a comprehensive overview of the main reservoirs and mechanisms accounting for the contrasting variability of radiogenic isotope systematics in the sub-oceanic mantle and the relative homogeneity of its volcanic products, highlighting the paradigm change promoted by the use of Hf isotopes. Secondly, we summarize the different models invoked to explain the decoupling/(re-)coupling of Hf and Nd isotopes. Decoupling above the mantle array is often related to melt-peridotite interaction involving ancient protoliths, whereas coupled Hf-Nd or decoupling below the array are shown to be insufficient criteria to exclude the involvement of such protoliths. The Hf-Nd isotope variability of the SCLM is then addressed using a tectono-thermal classification based on the Global Lithospheric Architecture Mapping (GLAM) project. The extreme variability that characterizes the cratonic SCLM reflects the long-term preservation of depleted signatures overprinted by ancient and recent metasomatic episodes. Refertilized SCLM domains fingerprinted by variably decoupled Hf-Nd isotope systematics record subduction-related processes, which also appears to be instrumental in the recycling of continental material into the convective mantle. We show that there is a critical "chicken-and-egg" question underpinning debates on the spatio-temporal evolution of the SCLM: whether ancient signatures are pre-existing in the lithosphere (*e.g.* "lithospheric memory" during refertilization) or introduced into the convective mantle (*i. e.* recycling). Importantly, our compilation shows that fertile lithologies such as pyroxenites can also carry extremely depleted isotopic signatures. In particular, delamination of gravitationally unstable, pyroxenite-rich arc roots represents a volumetrically significant flux of material characterized by ancient radiogenic Hf and basalt-like Nd-isotope compositions that can, once recycled, account for the Hf variability observed between MORB suites. In this context, the characteristic HIMU-like or coupled Hf-Nd signatures observed in garnet-pyroxenite layers from orogenic peridotite massifs probably reflects long-term processing (re-coupling) of recycled lithospheric material in the convective mantle. In contrast, continental dispersal during rifting (± plume-related processes) appears to be mostly limited to buoyant SCLM remnants in the oceanic lithosphere, and these are unlikely to be recycled unless previously refertilized. This work brings a new geodynamic perspective to the ancient signatures identified as chemical and isotopic heterogeneities in the oceanic lithosphere and convective mantle. These conclusions imply that (1) subduction is the main driver of mass transfer between lithosphere and asthenosphere and (2) the long-term evolution of the Earth's mantle and crust are directly linked to convergent plate-tectonic processes, at least since the Archean.

1. Introduction

The compositional evolution of the Earth's mantle *via* partial melting and subsequent magmatic processes is directly linked to the global differentiation of the planet in response to its long-term cooling (Zindler and Hart, 1986; Hofmann, 1988). Generation and recycling of the

* Corresponding author.
E-mail address: romain.tilhac@csic.es (R. Tilhac).

https://doi.org/10.1016/j.chemgeo.2022.121039
Received 22 February 2022; Received in revised form 21 June 2022; Accepted 21 July 2022
Available online 30 July 2022

oceanic lithosphere is a first-order control on the heterogeneity of the mantle (*e.g.*Jones et al., 2019), but recycling of continental material is also required to explain the enriched mantle components identified from the compositional variability of mid-ocean ridge (MORB) and ocean-island (OIB) basalts (Willbold and Stracke, 2010; Stracke, 2012). These processes represent a large-scale cycling between the Earth's major lithophile-element reservoirs. However, there is no consensus on the tectonic nature (*e.g.* delamination, rifting, sediment subduction, subduction erosion) of the dominant re-enrichment mechanism associated with this recycling (see Stracke, 2012, for a review).

In addition, extremely depleted isotopic signatures, undocumented in oceanic lavas, have been observed in abyssal peridotites (AP), revealing the existence of old residual domains that question the genetic relationships between oceanic mantle and crust (Salters and Dick, 2002; Cipriani et al., 2004; Alard et al., 2005; Warren et al., 2009; Stracke et al., 2011). Whether these domains represent depleted asthenosphere or more recently incorporated ancient sub-continental lithospheric mantle (SCLM) has been highly debated (*e.g.*Liu et al., 2008; O'Reilly et al., 2009; Griffin et al., 2012; Liu et al., 2022). Fundamental questions regarding the distribution of mantle heterogeneities and the efficiency of the processes (*i.e.* convection, deformation, recrystallization, diffusion, melt generation, transport and mixing) that can erase chemical and isotopic gradients underpin this issue (Rampone and Hofmann, 2012, and references therein). Studies showing that the isotopic variability of μm-scale melt inclusions exceeds that of erupted basalts (*e.g.*Saal et al., 1998; Stracke et al., 2019) question the paradigm in which partial melting takes place in local chemical equilibrium (Hofmann and Hart, 1978). They also highlight the fact that erupted lavas are mixtures of aggregated melt fractions and underestimate the heterogeneity of their source regions (*e.g.*Liu and Liang, 2017).

A comprehensive discussion of such considerations was provided 10 years ago by Rampone and Hofmann (2012) who reviewed evidence from AP and the Alpine-Apennines ophiolites, mainly from the perspective of Os and Sr-Nd isotopes as only few Hf-isotope data were available for mantle rocks at the time. Thanks to the popularization of multi-collector inductively coupled plasma mass spectrometry (MC-ICP-MS), the number of Hf-isotope analyses of mantle rocks has dramatically increased. Combined Hf-Nd studies in suites of MORB (Salters et al., 2011), AP (Stracke et al., 2011) and xenoliths (*e.g.*Bizimis et al., 2007; Byerly and Lassiter, 2014) have further documented the presence of depleted domains in the sub-oceanic mantle. However, the tectonic origin of such domains remains as a major unresolved issue essential to understanding the role of mantle heterogeneities and the long-term evolution of the continental crust (Jones et al., 2019, and references therein).

To address this issue, we present the first global review of Hf-Nd isotopes in the mantle, describing the current state of knowledge on the mantle's internal processes and recycling in both oceanic and continental environments. This review provides (1) an exhaustive compilation of Hf-Nd isotope data on peridotites and pyroxenites, (2) an overview of the isotopic variability of the sub-oceanic mantle as seen in peridotites and lavas, (3) a summary of the mechanisms explaining the ubiquitous decoupling of Hf and Nd isotopes, and (4) new geodynamic perspectives on the origin of isotopically depleted signatures based on the variability of the SCLM and the tectonic processes associated with continental recycling. To that end, we use an independent classification based on the systematics of the Global Lithospheric Architecture Mapping (GLAM) project which discriminates SCLM localities based on multi-disciplinary geodynamic considerations (Begg et al., 2009).

2. Data collection

2.1. Data sources and systematics

We have compiled Sm-Nd and Lu-Hf isotopic data published between 1995 and 2021 on mantle lithologies from 55 different regions and 121 localities worldwide (Fig. 1). As detailed in Tables 1a and 1b, this dataset includes:

- *Abyssal and ophiolitic peridotites* – Data are mostly from clinopyroxene (cpx) and whole-rock (WR, or reconstructed bulk-rock) aliquots, dominantly from spinel and/or plagioclase-facies peridotites.
- *Orogenic peridotite massifs* – Peridotites and pyroxenites are equally represented, mostly from the spinel-stability field, but also including garnet- and plagioclase-bearing samples. Data are from cpx and WR aliquots, and a few garnets from Beni Bousera pyroxenites.
- *Basalt-borne xenoliths* – The vast majority of these samples are spinel-facies (and a few garnet-facies) peridotites. Data are dominated by cpx with very few garnets and fewer WR data.
- *Kimberlite-borne xenoliths* – These samples are mostly garnet-facies peridotites with a sizeable proportion of pyroxenites. Garnet, cpx and WR data are abundant; data also include a few other phases such as orthopyroxene (opx) and amphibole.

Garnet-pyroxenite xenoliths from dioritic intrusions in the North China Craton and a suite of xenoliths hosted in basaltic trachyandesite from the Kharchinsky volcano in Kamchatka have also been included.

The dataset includes 1285 Lu-Hf and 1503 Sm-Nd analyses for a total of 1122 combined Hf-Nd analyses (Fig. 2) from either WR or reconstructed bulk rocks (when published), cpx, opx, garnet or accessory minerals. Garnet and cpx are the main major host minerals for Nd and Hf in the mantle with concentrations mostly in the range of 0.01–15 (up to $\sim$50) ppm Nd and 0.001–2 (up to $\sim$8) ppm Hf in cpx, and 0.01–5 (up to $\sim$20) ppm Nd and 0.02–1.5 (up to $\sim$2.5) ppm Hf in garnet (Fig. 3a). Both parent/daughter (P/D) ratios tend to be higher and more variable in garnet. $^{176}Lu/^{177}Hf$ ranges from 0.05–0.5 to >10 in garnet whereas cpx exhibits values <0.15 and down to <0.001; $^{147}Sm/^{144}Nd$ is restricted to 0.01–0.5 in cpx and garnet data are more dispersed (Fig. 3b). Several studies have emphasized the potential importance of opx and olivine in this budget for depleted peridotites and particularly cpx-free harzburgites (Salters and Zindler, 1995; Ionov et al., 2005b; Choi et al., 2010; Stracke et al., 2011; Choi and Mukasa, 2012; Doucet et al., 2015; Liu et al., 2020), but few data are available. The relative sensitivity of opx (and WR) to metasomatism compared to cpx has also been pointed out (Byerly and Lassiter, 2015).

Only the measured elemental concentrations (Sm, Nd, Lu, Hf), P/D ratios ($^{147}Sm/^{144}Nd$, $^{176}Lu/^{177}Hf$) and isotopic ratios ($^{143}Nd/^{144}Nd$, $^{176}Hf/^{177}Hf$) have been taken from the referenced papers. When not provided, P/D ratios were calculated from elemental concentration ratios. For consistency, all calculations were performed based on a single set of decay constants and accepted values (Table 2). The whole dataset (including Rb-Sr data when available) with sample details and references is provided in Electronic Appendix 1. Technical considerations are provided in Electronic Appendix 2. Note that we focus mostly on present-day isotopic compositions in order to discuss the origin of ancient components in the modern sub-oceanic mantle. Geochronological considerations are nonetheless provided in Electronic Appendix 3.

2.2. Tectono-thermal classification

Localities from the SCLM have been classified based on the systematics developed by the Global Lithospheric Architecture Mapping (GLAM) project, a worldwide 4D mapping of the lithospheric mantle discriminated into coherent tectonic blocks based on a multi-disciplinary approach including gravity, magnetics, seismic tomography, crustal seismic profiles, magnetotellurics and geochronological data (Begg et al., 2009). Using a terminology initially formulated by Janse (1994), the GLAM approach distinguishes *Archons (A)* with strongly depleted SCLM and the last major crustal events documented at >2.5 Ga (Griffin et al., 2009), *Protons (P)* with moderately depleted SCLM and major crustal events at 2.5–1.0 Ga, and *Tectons (T)*, with mildly depleted SCLM and major crustal events at <1.0 Ga. In addition,

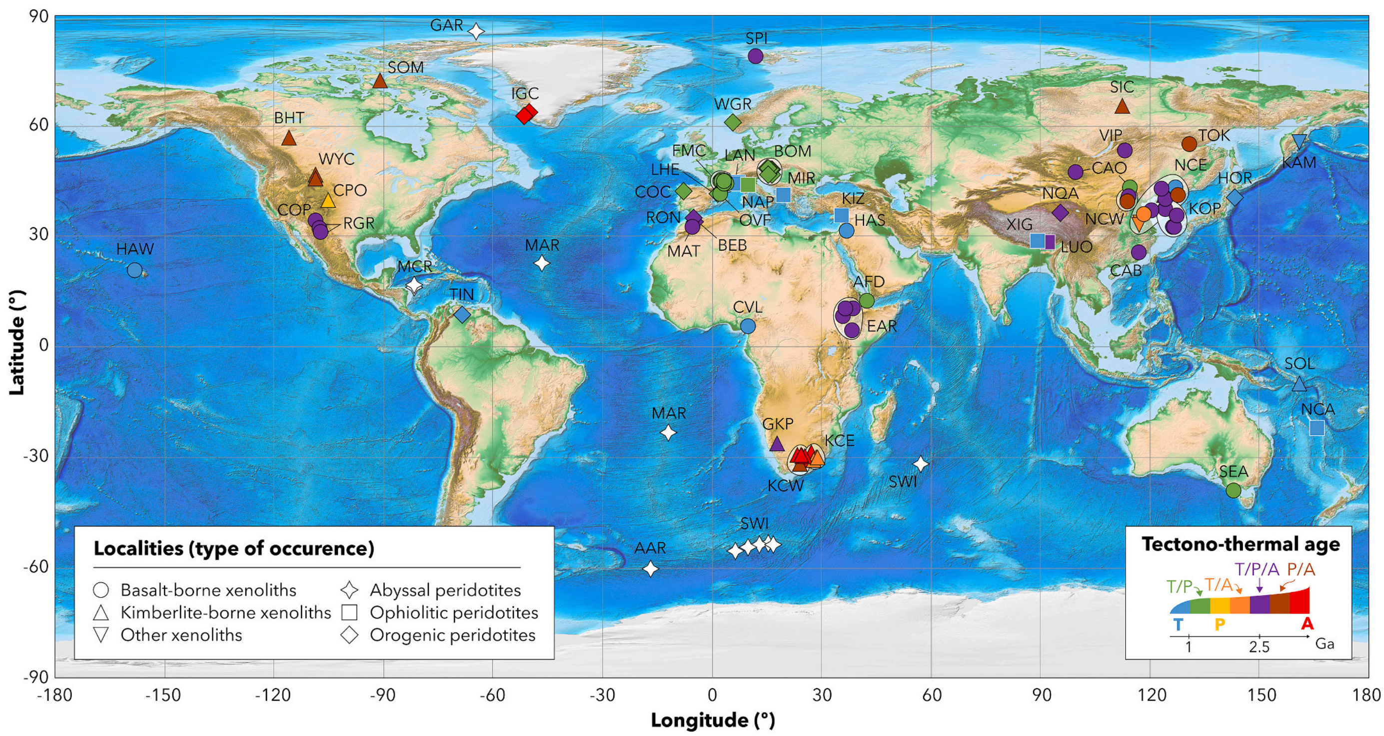

Fig. 1. Localities included in this compilation distinguished by type of occurrence and tectono-thermal age of the corresponding terrane. Abbreviations are indicated in Tables 1a and 1b. The coordinates of all the localities are provided in Electronic Appendix 1 and as KML file. See text for further information on the tectono-thermal classification. The background image is a global relief model of the Earth's surface from the NOAA National Centers for Environmental Information (doi: https://doi.org/10.7289/V5C8276M).

an Archon is referred to as *Proton/Archon (P/A)* if reworked at 2.5–1.0 Ga, *Tecton/Archon (T/A)* if reworked at <1 Ga or *Tecton/Proton/Archon (T/P/A)* if also reworked >1 Ga. The same reasoning applies to a reworked Proton, referred to as *Tecton/Proton (T/P)*. We thereafter refer to P/A, T/P/A and T/A as reworked Archean, as opposed to preserved Archean domains (A), to P and T/P simply as Proterozoic and to T as "recent" SCLM domains. This classification generally excludes plume-related magmatic episodes that are mostly thought not to have pervasive consequences throughout lithospheric blocks although they may be locally important – see for instance Bianchini et al. (2014) and Alemayehu et al. (2017).

Most reworked Archean domains included in this review are classified as T/P/A (Tables 1a and 1b). This is the case for orogenic massifs such as Ronda in Spain, Beni Bousera in Morocco and North Qaidam in Tibet, for Luobusa ophiolite in Tibet and for many basalt-borne xenoliths, particularly those from the Central Asian Orogenic Belt, the East African and Rio Grande rifts, the Korean Peninsula, and several localities on the North China Craton (NCC). The rest of the NCC localities and several kimberlite-borne xenolith suites (*e.g.* Buffalo Head Terrane in Canada or the Wyoming Craton) are classified as P/A (or T/A, as many of the eastern Kaapvaal Craton localities). Note that T/A localities are the least represented (Tables 1a and 1b), suggesting that Archean terranes that have not been reworked during the early- to mid-Proterozoic have mostly been preserved. Conversely, ~75% of Archean terranes reworked during the early- to mid-Proterozoic were also affected during the last 1 Gy (*i.e.* T/P/A). These observations may reflect the "accessibility" of pristine Archean lithosphere to arc magmas in the early Proterozoic, whereas subsequent subduction zones developed away from Archean continental cores, thus affecting already modified lithosphere.

Most early- to mid-Proterozoic terranes included in this study also show evidence of reworking at <1 Ga (*i.e.* T/P), except for Sloan in the Central Plains Orogen of western USA (Tables 1a and 1b). They include orogenic massifs such as the Bohemian Massif in Czech Republic, the Cabo Ortegal Complex in Spain, Lherz in France and the Western Gneiss Region in Norway, as well as basalt-borne xenoliths (*e.g.* French Massif Central, SE Australia). In contrast, all the ophiolites (except Rio Strega in the Northern Apennines, Italy) along with Tinaquillo in Venezuela and Horoman peridotites in Japan are classified as T. This is also the case for basalt-borne xenoliths from Hawaii, Nyos in the Cameroon Volcanic Line, Jiaohe in the Central Asian Orogen, Harrat Ash Shaam in the northern Arabian Peninsula, and those from the Malaita alnöite in the Solomon Islands and basaltic trachyandesite dykes of the Karchinsky volcano in Kamtchatka.

3. Compositional variability of the sub-oceanic mantle

3.1. Background information on the Sm-Nd and Lu-Hf systems

The decay of ^{176}Lu by β^- emission to ^{176}Hf, with a half-life of 37.1 Ga (Scherer et al., 2001), has been widely used in isotope geochemistry and geochronology since its development by Patchett and Tatsumoto (1980a, 1980b) who first overcame the poor ionization efficiency of Hf by Thermal Ionization Mass Spectrometry (TIMS) – see also Vervoort (2014). During partial melting of the mantle, the behaviour of the Lu-Hf isotopic system is comparable to that of Sm-Nd. Both systems are based on lithophile rare-earth-element (REE) parents that are more compatible than their daughters. However, the Lu-Hf system is more robust to tectono-thermal perturbation (*e.g.*Vervoort and Blichert-Toft, 1999; Gonzaga et al., 2010), because its closure temperatures are probably higher than those of Sm-Nd (see Blichert-Toft et al., 1999; Scherer et al., 2000; Cheng et al., 2008; Shu et al., 2014 for cpx-garnet pairs). Lutetium and Hf are also much less readily affected by fluid interaction than Sm and Nd. As a high-field-strength element (HFSE), Hf preferentially partitions into zircon and Ti-rich minerals (Fujimaki, 1986; Foley et al., 2000), whereas Lu preferentially enters garnet (*e.g.*Johnson, 1998). Magmatic and metasomatic processes involving fluids and/or leading to modal changes in the above minerals (as well as metamorphic and sedimentary processes) are thus able to decouple the two systems.

Table 1a
Abyssal, ophiolitic and orogenic peridotite localities.

Location & sample details					Global Lithospheric Architecture Mapping (GLAM)			References	
	Region	Locality	Lithology	Facies	Environment	Tectono-thermal age	Arc/ back-arc events	Sm-Nd isotopes	Lu-Hf isotopes
ABYSSAL PERIDOTITES									
AAR	American Antarctic Ridge	59°S Fracture Zone (NW wall)	Lherzolite	Spinel				Snow (1993), Stracke et al. (2011)	Salters and Zindler (1995), Stracke et al. (2011)
GAR	Gakkel Ridge	Rift wall	Lherzolite, Harzburgite	Spinel				Stracke et al. (2011)	Stracke et al. (2011)
MAR	Mid Atlantic Ridge	22°S Fracture Zone, Kane Fracture Zone	Lherzolite, Peridotite, Harzburgite	Plagioclase, Spinel				Frisby et al. (2016b), Mallick et al. (2014)	Frisby et al. (2016b)
MCR	Mid Cayman Rise	Alvin dive, Eastern rift wall (18.17°N), Eastern rift wall (18.21°N)	Lherzolite, Harzburgite	Plagioclase, Spinel				Mallick et al. (2014), Frisby et al. (2016b)	Frisby et al. (2016b)
SWI	South West Indian Ridge	Abyssal Hills (SE Islas Orcadas FZ), Atlantis II Fracture Zone (N. RTI corner), Axial trough (15.23°E), Dingaan Fracture Zone (NW wall), Fault scarp (16.64°E), Shaka Fracture Zone (E. inside corner)	Lherzolite, Peridotite, Harzburgite	Spinel, Plagioclase, Plagioclase/spinel				Stracke et al. (2011), Snow (1993), Mallick et al. (2014), Frisby et al. (2016a), Frisby et al. (2016b)	Stracke et al. (2011), Salters and Zindler (1995), Frisby et al. (2016b), Mallick et al. (2015)
OPHIOLITIC PERIDOTITES									
KIZ	Kizildag		Harzburgite, Pyroxenite	Spinel	Arc-related	T	1	Liu et al. (2020)	Liu et al. (2020)
LAN	Lanzo (north)		Harzburgite, Lherzolite	Spinel, Plagioclase/spinel	Marginal	T		Guarnieri et al. (2012)	Guarnieri et al. (2012)
	Lanzo (south)		Harzburgite	Spinel, Plagioclase	Marginal	T		Sanfilippo et al. (2019)	Sanfilippo et al. (2019)
LUO	Luobusa		Lherzolite, Harzburgite	Spinel	Arc-related	T/P/A	5	Zhang et al. (2020)	Zhang et al. (2020)
MIR	Mirdita		Pyroxenite	Garnet	Marginal	T	1	Gjata et al. (1992)	Blichert-Toft et al. (1999)
NCA	New Caledonia	Ouassë Bay	Websterite	Spinel	Oceanic	T		Xu et al. (2021)	Xu et al. (2021)
NAP	Northern Apennine	Rio Strega, Rio Parola, Monte Prinzera, Valceno quarry	Clinopyroxenite, Pyroxenite, Peridotite, Websterite	Garnet, Spinel/ garnet, Spinel, Plagioclase-spinel	Continental	T/P	1	Montanini et al. (2006), Montanini et al. (2012), Montanini and Tribuzio (2015)	Montanini et al. (2006), Montanini et al. (2012), Montanini and Tribuzio (2015)
XIG	Xigaze		Harzburgite, Lherzolite	Spinel	Arc-related	T	1		Liu et al. (2020)
OROGENIC MASSIFS									
BEB	Beni Bousera		Clinopyroxenite, Websterite, Pyroxenite	Garnet, Spinel, Spinel/garnet	Arc-related	T/P/A	1	Pearson and Nowell (2004), Blichert-Toft et al. (1999), Varas-Reus et al. (2018)	Pearson and Nowell (2004), Blichert-Toft et al. (1999), Varas-Reus et al. (2018)
BOM	Bohemian Massif	Bečváry, Biskupice, Doubrava, Horní Kounice, Karlstetten, Meidling, Mohelno, Níhov, Nové Dvory, Úhrov	Clinopyroxenite, Lherzolite, Websterite	Garnet, Spinel/ garnet, Spinel	Arc-related	T/P	2	Svojtka et al. (2016), Medaris et al. (1995), Ackerman et al. (2020), Beard et al. (1992)	Ackerman et al. (2016), Ackerman et al. (2020)
COC	Cabo Ortegal Complex	Herbeira	Clinopyroxenite, Websterite, Olivine clinopyroxenite, Hornblendite, Orthopyroxenite, Harzburgite	Spinel, Garnet, Spinel/garnet	Arc-related	T/P	2	Tilhac et al. (2017), Santos et al. (2002)	Tilhac et al. (2020)
HOR	Horoman		Lherzolite, Harzburgite	Plagioclase, Spinel	Marginal	T	1	Yoshikawa and Nakamura (2000), Takazawa et al. (1995), Takazawa (1996), Malaviarachchi et al. (2008)	Malaviarachchi et al. (2008)
IGC		Isua, Narssaq	Peridotite, Harzburgite, Dunite	Spinel	Continental	A	1	van de Löcht et al. (2020)	van de Löcht et al. (2020)

(*continued on next page*)

Table 1a (*continued*)

Location & sample details					Global Lithospheric Architecture Mapping (GLAM)			References	
	Region	Locality	Lithology	Facies	Environment	Tectono-thermal age	Arc/ back-arc events	Sm-Nd isotopes	Lu-Hf isotopes
	Itsaq Gneiss Complex								
LHE	Lherz		Lherzolite, Harzburgite	Spinel	Marginal	T/P		Le Roux et al. (2009)	Le Roux et al. (2009)
NQA	North Qaidam	Shenglikou	Clinopyroxenite	Garnet	Arc-related	T/P/A	2	Xiong et al. (2014)	Xiong et al. (2014)
RON	Ronda		Pyroxenite	Garnet	Arc-related	T/P/A	1	Varas-Reus et al. (2018)	Varas-Reus et al. (2018)
TIN	Tinaquillo		Hornblendite, Lherzolite	Spinel	Marginal	T	1	Choi et al. (2007)	Choi et al. (2007)
WGR	Western Gneiss Region	Sandvik	Lherzolite, Websterite, Olivine pyroxenite	Garnet	Marginal	T/P		Lapen et al. (2005)	Lapen et al. (2005)

Oceanic refers to mid-ocean ridge and intra-oceanic settings; *Continental* refers to orogenic, post-orogenic, intra-continental, continental rift, intra-cratonic, intra-cratonic rift, craton margin and micro-continental settings; *Marginal* refers to passive margin, marginal basin, continental margin and accretionary prism settings; *Arc-related* refers to back-arc basin, back-arc/continental, magmatic arc, continental arc and forearc settings. The number of arc/back-arc events corresponds to the number of events before the age of eruption/emplacement. T, Tecton; P, Proton; A, Archon; T/P, Tecton/Proton; T/P/A, Tecton/Proton/Archon; T/A, Tecton/Archon; T/P, Tecton/Proton. See text for further detail on this classification. Note that data from Borghini et al. (2021) and Sanfilippo et al. (2022) are not included as they were published while this review was in final stages of preparation.

Benefiting from these complementary characteristics, the combined application of Hf-Nd isotopes has significantly contributed to our understanding of the evolution of the Earth's crust-mantle system (Vervoort and Blichert-Toft, 1999; Chauvel et al., 2008; Stracke, 2012; Gardiner et al., 2019; Jones et al., 2019).

$^{143}Nd/^{144}Nd$ and $^{176}Hf/^{177}Hf$ are well correlated in OIB (Patchett and Tatsumoto, 1980a; Patchett, 1983), defining with MORB the *mantle array* (Fig. 4a), which nearly parallels the *terrestrial array* that also includes juvenile continental rocks and sediments (Vervoort et al., 1999; Vervoort et al., 2011). As for Nd, Hf-isotope compositions are normalized to the Bulk Silicate Earth (BSE), which is estimated from the Chondritic Uniform Reservoir (CHUR; Table 2) based on high-precision analyses of chondrites (Blichert-Toft and Albarède, 1997), using the ε notation:

$$\varepsilon_{Hf} = \left[\left(\frac{^{176}Hf}{^{177}Hf} \right)_{sample} \Big/ \left(\frac{^{176}Hf}{^{177}Hf} \right)_{BSE} - 1 \right] \times 10^4$$

The mantle array based on the basalt compilation of Chauvel et al. (2008) has a slope of $\varepsilon_{Hf} = 1.59\ \varepsilon_{Nd}$, lying 1.28 ε units above the BSE value of $^{176}Hf/^{177}Hf = 0.282772 \pm 29$ (Blichert-Toft and Albarède, 1997) and up to 3 ε units depending on the authors (Table 3). On this basis, it was postulated that the primitive mantle (PM) sampled by OIB was not completely undifferentiated and that a *missing component* was needed in addition to the depleted mantle (DM) and continental crust to account for the BSE (Blichert-Toft and Albarède, 1997; Albarède et al., 2000). Potential candidates have included subducted oceanic crust (Blichert-Toft and Albarède, 1997; Bizzarro et al., 2002), lower continental crust (Vervoort et al., 2000) or the SCLM (Griffin et al., 2000), and early differentiation of the chondritic Earth *via* perovskite removal from a magma ocean (Blichert-Toft and Albarède, 1997). However, as long suspected (Salters and White, 1998; Vervoort et al., 1999), the most recent estimate of $^{176}Hf/^{177}Hf = 0.282785 \pm 11$ for the BSE (Bouvier et al., 2008) is within error of the Hf-Nd mantle array (Tables 2 & 3).

As summarized in Fig. 4a, the isotopic variability of oceanic basalts along the Hf-Nd mantle array can be described by a DM component, mostly documented in MORB, and slightly more enriched compositions abundant in OIB, known as the prevalent mantle (PREMA; Zindler and Hart, 1986) or focal zone (FOZO; Hart et al., 1992) – see Stracke et al. (2005) for discussion of these acronyms. To a first order, variability within the DM-PREMA range can be accounted for by the production and recycling of oceanic crust (Stracke, 2012). In addition, most OIB suites extend towards less radiogenic Nd- and Hf-isotope compositions, defining enriched-mantle (EM) components *sensu stricto*.

Relating *isotopic components* identified in basalt suites to actual *mantle components* (*i.e.* mineralogically distinct parts of the mantle) and identifying the geological processes that produced and mixed these components is not straightforward (see for instance Armienti and Gasperini, 2007). A long-prevailing view holds that crustal recycling produces discrete enriched domains in the mantle, the mixing of which then leads to the isotopic variability in OIB (Zindler and Hart, 1986). If mixing occurs solely *via* convection stirring (*i.e.* in solid state), this view requires a rather selective mixing to produce the observed linear EM trends (Fig. 4a). However, because the length scale of mantle heterogeneities is most likely smaller than that of the melting region, EM components can also be mixed during melting (Stracke, 2012) so that their relative contribution can vary as well as their distribution (Allègre et al., 1984; Ito and Mahoney, 2005). Stracke (2012) showed that OIB and MORB formed by low degrees of melting, as well as continental volcanics, all preferentially sample PREMA, suggesting that the latter is petrologically distinct from the DM (*i.e.* more fertile).

3.2. Recycling of enriched components

In contrast to the Sm-Nd system, the Lu-Hf system is strongly fractionated between sandstones and clays due to the strong affinity of Hf for

Table 1b
Basalt- and kimberlite-borne xenolith localities.

Location & sample details					Global Lithospheric Architecture Mapping (GLAM)			References	
	Region	Locality	Lithology	Facies	Environment	Tectono-thermal age	Arc/back-arc events	Sm-Nd isotopes	Lu-Hf isotopes
BASALT-BORNE XENOLITHS									
AFD	Afar Depression	Mt El Taghi	Lherzolite, Olivine websterite, Dunite	Spinel, Plagioclase/spinel	Continental	T/P	2	Teklay et al. (2010)	Teklay et al. (2010)
CVL	Cameroon Volcanic Line	Nyos	Lherzolite, Harzburgite	Spinel	Continental	T		Liu et al. (2019), Liu et al. (2017a)	Liu et al. (2019), Liu et al. (2017a)
CAB	Cathaysia Block	Mingxi (Dayangke)	Lherzolite, Harzburgite	Spinel, Garnet	Arc-related	T/P/A	2	Liu et al. (2017b)	(Liu et al., 2017b)
CAO	Central Asian Orogen	Abaga, Jiaohe (Yiqisong), Shuangliao (Bobotushan), Shuangliao (Bolishan), Tariat (Haer), Tariat (Shavaryn-Tsaram), Tariat (Zala)	Harzburgite, Lherzolite, Olivine websterite, Websterite	Spinel	Continental, Arc-related	T, T/P, T/P/A	2, 3, 5	Zhang et al. (2012), Yu et al. (2009), Carlson and Ionov (2019)	Zhang et al. (2012), Yu et al. (2009), Carlson and Ionov (2019)
COP	Colorado Plateau	Cerro Chato	Lherzolite	Spinel	Arc-related	T/P/A	4	Byerly and Lassiter (2012), Byerly and Lassiter (2015)	Byerly and Lassiter (2015)
EAR	East African Rift	Dedessa, Injibara, Mega	Lherzolite, Olivine websterite, Harzburgite	Spinel	Continental	T/P/A	2	Beccaluva et al. (2011)	Bianchini et al. (2014)
	Ethiopian Plateau	Gundeweyn	Lherzolite	Spinel	Continental	T/P/A		Alemayehu et al. (2017)	Alemayehu et al. (2017)
HAS	Harrat Ash Shaam		Peridotite, Pyroxenite	Spinel, Spinel/garnet	Continental	T	2	Shaw et al. (2007)	Shaw et al. (2007)
HAW	Hawaii	Oahu (Kaau), Oahu (Pali), Oahu (Salt Lake Crater)	Lherzolite, Clinopyroxenite	Spinel, Garnet	Oceanic	T		Bizimis et al. (2003), Bizimis et al. (2005), Salters and Zindler (1995)	Bizimis et al. (2003), Bizimis et al. (2005), Salters and Zindler (1995)
KOP	Korean Peninsula	Baengnyeong Island, Jeju Island (Sangumburi), Jeju Island (Sinsanri), Jogokni	Lherzolite, Harzburgite, Clinopyroxenite, Megacryst	Spinel	Arc-related, Continental	T/P/A	2, 3, 4	Choi et al. (2005), Choi and Mukasa (2012)	Choi and Mukasa (2012)
FMC	Massif Central (north)	Fraisse, Les Champs, Montboissier, Puy Beaunit, Puy de la Hale, Sauterre, Zanières	Harzburgite, Lherzolite	Spinel	North China Craton (NCC) - East	T/P	2	Downes et al. (2003), Downes and Dupuy (1987)	Wittig et al. (2006), Wittig et al. (2007)
	Massif Central (south)	Maar de Borée, Monistrol d'Allier, Mont Briançon, Ray Pic, Tarreynes	Lherzolite, Harzburgite, Wehrlite	Spinel	Arc-related	T/P	2	Zangana et al. (1997), Downes and Dupuy (1987)	Wittig et al. (2007), Wittig et al. (2006)
MAT	Middle Atlas		Lherzolite, Harzburgite	Spinel	Marginal	T/P/A	1	Wittig et al. (2010)	Wittig et al. (2010)
NCW	North China Craton (west)	Kuandian, Mt. Baekdu, Penglai, Shanwang	Harzburgite, Lherzolite, Wehrlite, Pyroxenite	Spinel	Continental, Arc-related	T/A, P/A, T/P/A	2, 3	Wu et al. (2006), Park et al. (2017), Chu et al. (2009)	Wu et al. (2006), Park et al. (2017), Chu et al. (2009)
NCE	North China Craton (east)	Hannuoba, Sanyitang, Yangyuan	Lherzolite, Websterite, Harzburgite	Spinel	Arc-related	P/A, T/P/A	3	Choi et al. (2008), Zhao et al. (2021), Liu et al. (2012), Yang et al. (2018)	Choi et al. (2008), Zhao et al. (2021), Liu et al. (2012), Yang et al. (2018)
OVF	Olot Volcanic Field		Harzburgite, Lherzolite	Spinel	Continental	T/P		Bianchini et al. (2007)	Bianchini et al. (2007)
RGR	Rio Grande Rift	Elephant Butte, Kilbourne Hole, Potrillo Maar	Lherzolite, Harzburgite	Spinel	Arc-related	T/P/A	3	Byerly and Lassiter (2012), Byerly and Lassiter (2014), Byerly and Lassiter (2015), Salters and Zindler (1995)	Byerly and Lassiter (2014), Byerly and Lassiter (2015), Salters and Zindler (1995)
SEA	Southeastern Australia	Lakes Bullenmerri/Gnotuk	Websterite, Clinopyroxenite	Garnet	Continental	T/P	2	Lu et al. (2018), Lu et al. (2020)	Lu et al. (2018), Lu et al. (2020)
SPI	Spitsbergen	Svalbard (Sverrefjell)	Lherzolite, Harzburgite	Spinel	Continental	T/P/A	1	Choi et al. (2010)	Choi et al. (2010)
TOK	Tokinsky Stanovik		Lherzolite, Harzburgite, Olivine clinopyroxenite	Spinel	Continental	P/A	2	Ionov et al. (2006)	Ionov et al. (2006)

(*continued on next page*)

Table 1b (*continued*)

Location & sample details					Global Lithospheric Architecture Mapping (GLAM)			References	
	Region	Locality	Lithology	Facies	Environment	Tectono-thermal age	Arc/back-arc events	Sm-Nd isotopes	Lu-Hf isotopes
VIP	Vitim Plateau		Composite peridotite, Lherzolite	Garnet, Spinel/garnet, Spinel	Arc-related	T/P/A	1	Ionov et al. (2005a)	Ionov et al. (2005b)
KIMBERLITE-BORNE XENOLITHS									
BHT	Buffalo Head Terrane	Buffalo Head Terrane	Lherzolite, Websterite, Harzburgite	Spinel, Garnet, Spinel/garnet	Arc-related	P/A	2	Aulbach et al. (2004)	Aulbach et al. (2004)
CPO	Central Plains Orogen	Sloan	Lherzolite, Harzburgite, Websterite	Spinel/garnet, Garnet, Spinel	Arc-related	P	2	Carlson et al. (2004)	Carlson et al. (2004)
GKP	Gibeon Kimberlite Province	Louwrencia	Peridotite	Garnet	Continental	T/P/A	1	Bedini et al. (2004)	Bedini et al. (2004)
KCE	Kaapvaal Craton (east)	Lace, Letseng-la Terai, Liqhobong, Matsoku, Taba Putsoa	Harzburgite, Lherzolite	Garnet, Spinel, Spinel/garnet	Continental	T/A*, A		Shu and Brey (2015), Shu et al. (2013), Simon et al. (2007), Bedini et al. (2004)	Shu and Brey (2015), Shu et al. (2013), Simon et al. (2007), Bedini et al. (2004)
KCW	Kaapvaal Craton (west)	Bellsbank, Bulfontein, De Beers, Finsch, Jagersfontein, Kamfersdam, Kimberley, Newlands, Roberts Victor, Roodekraal	Eclogite, Clinopyroxenite, Harzburgite, MARID, Websterite, Lherzolite, PIC, Wehrlite, Dunite	Garnet, Spinel	Continental	P/A, A	0, 1	Shu et al. (2014), Shu and Brey (2015), Fitzpayne et al. (2019), Gonzaga et al. (2010), Bedini et al. (2004), Simon et al. (2007), Fitzpayne et al. (2020), Giuliani et al. (2015), Lazarov et al. (2012b), Lazarov et al. (2012a), Shu et al. (2019), Lazarov et al. (2009), Shu et al. (2013)	Shu et al. (2014), Shu and Brey (2015), Fitzpayne et al. (2019), Gonzaga et al. (2010), Bedini et al. (2004), Simon et al. (2007), Fitzpayne et al. (2020), Giuliani et al. (2015), Lazarov et al. (2012b), Lazarov et al. (2012a), Shu et al. (2019), Lazarov et al. (2009), Shu et al. (2013)
NCE	North China Craton (east)	Tieling	Peridotite	Spinel	Continental	T/P/A	2	Wu et al. (2006)	
SIC	Siberian Craton	Udachnaya (East)	Lherzolite, Harzburgite	Garnet, Spinel	Continental	P/A		Doucet et al. (2015)	Doucet et al. (2015)
SOL	Solomon Islands	Malaita	Clinopyroxenite	Garnet	Oceanic	T		Ishikawa et al. (2007), Gonzaga et al. (2010)	Ishikawa et al. (2007), Gonzaga et al. (2010)
SOM	Somerset Island	Nikos	Lherzolite, Harzburgite, Peridotite, Websterite	Garnet, Spinel	Continental	P/A	2	Schmidberger et al. (2001)	Schmidberger et al. (2002)
WYC	Wyoming Craton	Homestead	Websterite, Harzburgite, Lherzolite	Spinel, Garnet	Marginal	P/A	1	Carlson et al. (2004)	Carlson et al. (2004)
OTHER XENOLITHS									
KAM	Kamtchatka arc	Karchinsky	Olivine websterite, Olivine clinopyroxenite, Clinopyroxenite, Dunite, Harzburgite,	Spinel		T	2	Siegrist et al. (2019)	Siegrist et al. (2019)
NCE	North China Craton (east)	Xuzhou-Suzhou (Jiagou, Liguo)	Clinopyroxenite	Garnet		T/A	2	Meng et al. (2019)	Meng et al. (2019)

(see Table 1a); * most east Kaapvaal localities (except Lace) are classified as T/A due to the impact of the Karoo LIP although plume-related events are not generally used as classifier in the GLAM at the regional scale. In some regions, localities with a different number of arc/back-arc events are indicated.

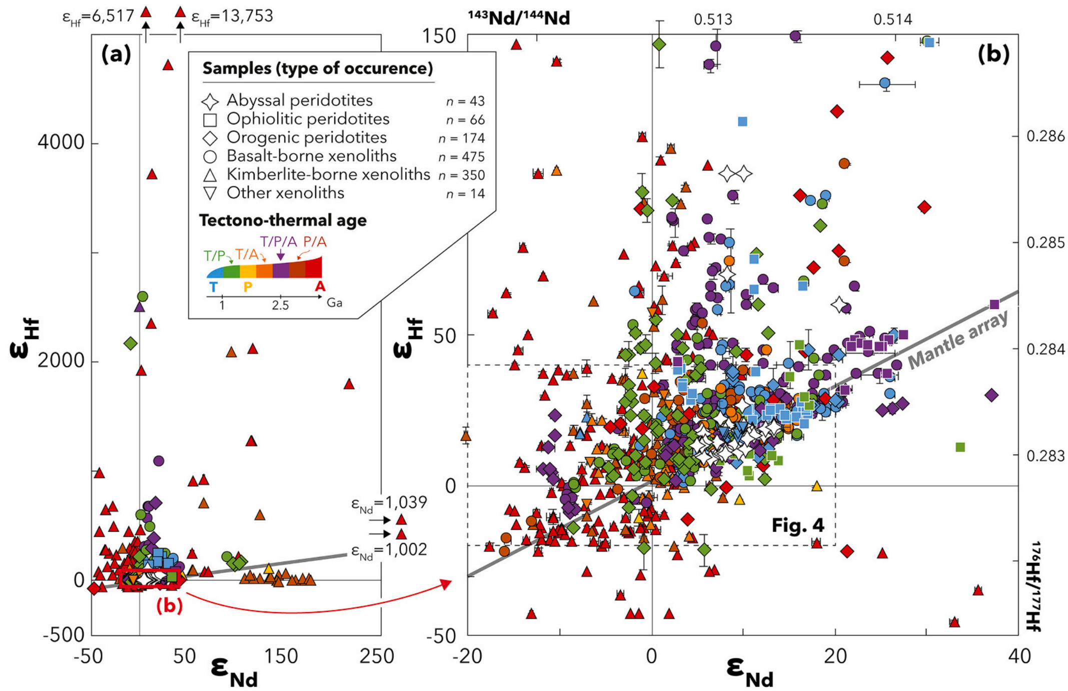

Fig. 2. Present-day Hf- and Nd-isotope compositions in ε_{Nd}-ε_{Hf} space for the whole dataset compiled in this review; symbols and colour coding as in Fig. 1. The full extent of isotopic variability is shown in (a) whereas the ε_{Nd}-ε_{Hf} space is restricted to ε_{Hf} − 50 to +150 and ε_{Nd} − 20 to +40 (b) where a significant proportion of the data is clustered. Error bars correspond to 2σ. Data sources are listed in Tables 1a and 1b. The grey line represents the mantle array of Chauvel et al. (2008) calculated as $\varepsilon_{Hf} = 1.59\ \varepsilon_{Nd} + 1.28$. For reference, $^{176}Hf/^{177}Hf$ and $^{143}Nd/^{144}Nd$ ratios are shown as secondary axes. The same dataset is plotted in $^{87}Sr/^{86}Sr$-ε_{Nd} space in Electronic Appendix Fig. A1.

zircon and the resistance of zircon to mechanical and chemical erosion (Patchett et al., 1984). The Hf-Nd isotopic systematics of sediments thus are sensitive to mineral sorting during continental weathering processes, transport and deposition (*e.g.*Garçon et al., 2013; Bayon et al., 2016; Corentin et al., 2022). As shown in Fig. 4a, terrigenous and pelagic sediments exhibit radiogenic Hf and plot slightly above the terrestrial array (Vervoort et al., 2011, and references therein). Their recycling into the mantle during subduction has long been thought to affect the compositions of magmas such as island-arc basalts (White and Patchett, 1984; Ben Othman et al., 1989; Chauvel et al., 2009; Yogodzinski et al., 2010; Handley et al., 2011; Waight et al., 2017), whose Hf and Nd isotope compositions overlap with the OIB field (Fig. 4a). Following this line of reasoning, inherited from Sr-Pb isotopic systematics, the slopes of the Hf-Nd mantle array and individual basalt suites have mostly been interpreted in terms of the nature and proportion of enriched components recycled as sediments and MORB (White et al., 1986; Chauvel et al., 1992; Vervoort et al., 1999; Chauvel et al., 2008).

In the global isotopic variability of OIB, enriched-mantle end members are represented by Pitcairn (EM1) and Samoan (EM2) basalts which, although poorly differentiated in ε_{Nd}-ε_{Hf} space (Fig. 4a), are characterized by higher $^{87}Sr/^{86}Sr$ and homogeneous $^{206}Pb/^{204}Pb$ for EM2. The variability observed in OIB with EM affinity can be regarded as a mixture of EM1 and EM2 mantle components (Stracke, 2012), in turn interpreted as recycled pelagic and terrigenous sediments, respectively (Zindler and Hart, 1986), or as derived from lower and upper continental crust (Willbold and Stracke, 2010). While the introduction of upper continental crust is compatible with the recycling of terrigenous sediments, the mechanism by which the lower continental crust might be recycled is debated (Stracke, 2012, and references therein; Tang et al., 2015). In addition, some OIB lavas have high $^{206}Pb/^{204}Pb$, requiring high time-integrated $^{238}U/^{204}Pb$ (μ). These so-called HIMU (for high-μ) lavas are depleted in fluid-mobile trace elements, have unradiogenic Sr isotopes and tend to plot below the Hf-Nd mantle array (Fig. 4a), but this pattern is not restricted to HIMU lavas (*e.g.* Azores lavas, Béguelin et al., 2017). No consensus exists on the origin and significance of HIMU basalts (Stracke et al., 2003) but they are mostly interpreted as reflecting the presence of subduction-modified oceanic crust ± sediments (Hofmann and White, 1980; Salters and White, 1998; Elliott et al., 1999). In contrast to the DM-PREMA and Pitcairn-like (EM1) components ubiquitous in OIB, MORB and continental volcanics, the distribution of HIMU and Samoa-like (EM2) components is very limited (Stracke, 2012). End-member HIMU basalts are rare, homogeneous and mostly restricted to St Helena, the Cook Austral islands and Mt. Erebus in Antarctica (Stracke et al., 2003, and references therein). This distribution is hard to reconcile with the fact that subduction operates globally and with the isotopic heterogeneity expected from subducted oceanic products (*e.g.*Béguelin et al., 2017).

3.3. *Records of ancient depletion*

3.3.1. *Hf-Nd isotope systematics in MORB*

The Hf- and Nd-isotope compositions of MORB are not as well correlated as those of OIB, which Patchett and Tatsumoto (1980a) attributed to stronger fractionation of Lu-Hf compared to Sm-Nd during partial melting. The radiogenic Hf-isotope compositions of MORB (*i.e.* positive ε_{Hf}) are also unsupported by their sub-chondritic present-day $^{176}Lu/^{177}Hf$. This so-called *Hf paradox* requires a mantle source with long-term depletion and high Lu/Hf (Salters and Hart, 1989). The Hf paradox of MORB and their slight HREE depletion (Shen and Forsyth, 1995) are interpreted as a *garnet signature* reflecting the presence of garnet in the source of these lavas (Salters, 1996). Such a signature, classically observed in OIB as a consequence of melting in the stability field of garnet peridotites (*e.g.*Niu et al., 2011), is debated in MORB because it implies a melt production exceeding the observed thickness of the oceanic crust. To reconcile these observations, the contribution of garnet pyroxenites allowing the presence of garnet at shallower depth (Hirschmann and Stolper, 1996) or the existence of a deep, hydrous region with low melting degrees ("low-F tail") have been invoked (*e.g.*

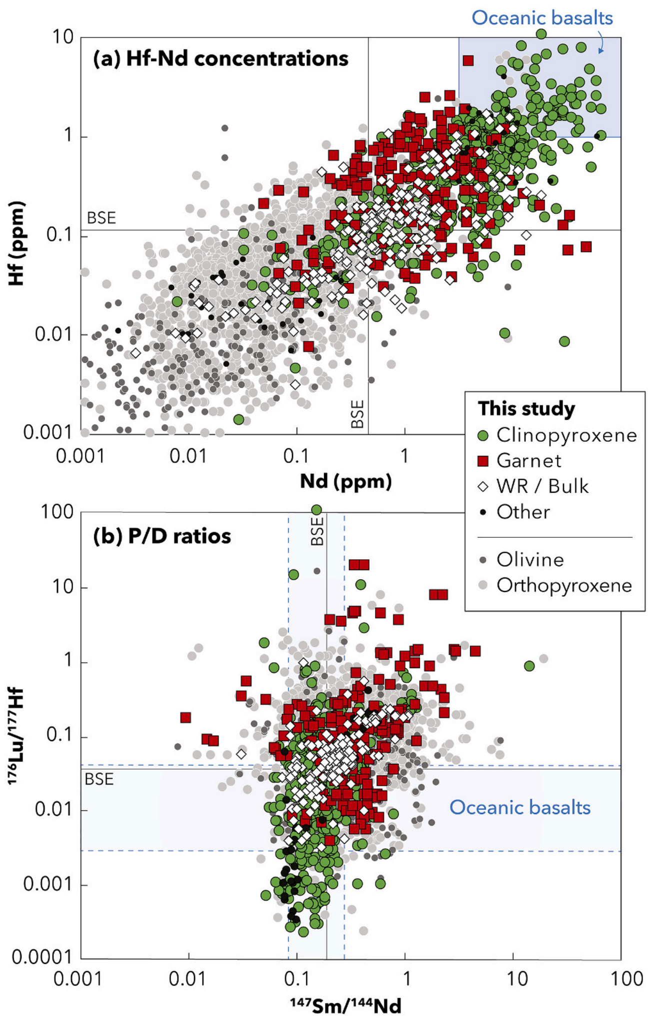

Fig. 3. Concentrations of Hf *vs* Nd (a) and parent/daughter (P/D) ^{176}Lu/^{177}Hf *vs* ^{143}Nd/^{144}Nd (b) in clinopyroxene, garnet and whole-rock or calculated bulk-rock samples included in this review; *Other* refers to other minerals as detailed in Electronic Appendix 1. Olivine and orthopyroxene from GeoRoc (http://georoc.mpch-mainz.gwdg.de/georoc/) are shown for comparison; only mantle lithologies (*i.e.* peridotites and pyroxenites) are included. Oceanic basalts (MORB and OIB) from GeoRoc are also shown. The BSE shown as reference lines correspond to the chondritic estimates of McDonough and Sun (1995).

Asimow and Langmuir, 2003). However, as pointed out by Chauvel and Blichert-Toft (2001), the Hf paradox of MORB may not require residual garnet depending on the set of partition coefficients and melting regime considered (Blundy et al., 1998). In fact, HREE depletion can be explained without invoking residual garnet if the relatively slow diffusivities of HREE are taken into account during basalt genesis (Van Orman et al., 2002; Oliveira et al., 2020).

In detail, individual MORB suites globally define an array of sub-parallel trends in ε_{Nd}-ε_{Hf} space. Hafnium and Nd isotopes are correlated at the mid-ocean ridge (MOR) segment scale (*i.e.* hundreds of km) but different segments have different Hf-isotope compositions (Fig. 4b). This observation may reflect large-scale variations in the MORB source inherited from various extents of garnet-present melting in ancient melting regimes (Salters et al., 2011). Alternatively, Salters et al. (2011) envisaged large-scale variations in the distribution of an ancient, depleted component with highly radiogenic Hf, previously unidentified in the convective mantle and interpreted as residual lithosphere after MORB extraction (*ReLish*). The sub-ridge mantle has recently been proposed to be volumetrically dominated by ReLish in a architecture where DM and EM only represent scattered pockets (Sanfilippo et al., 2019; Sanfilippo et al., 2021). However, because ReLish must combine radiogenic Hf and high Hf/Nd in order to produce a vertical spread in ε_{Nd}-ε_{Hf} space, its petrological nature and tectonic origin remains unclear.

Table 2
Constant parameters and reservoir compositions.

Decay constants		
λ_{Sm}	6.539×10^{-12} a^{-1}	Begemann et al. (2001)
λ_{Lu}	1.865×10^{-11} a^{-1}	Scherer et al. (2001)
Natural relative abundances		
^{147}Sm	0.1499	
^{144}Nd	0.238	
^{176}Lu	0.0259	
^{177}Hf	0.186	
Chondritic Uniform Reservoir (CHUR)		
^{147}Sm/^{144}Nd	0.196	Bouvier et al. (2008)
^{143}Nd/^{144}Nd	0.51263	Bouvier et al. (2008)
^{176}Lu/^{177}Hf	0.034	Bouvier et al. (2008)
^{176}Hf/^{177}Hf	0.282785	Bouvier et al. (2008)
Depleted Mantle (DM)		
^{147}Sm/^{144}Nd	0.214	Hofmann (2014)
^{143}Nd/^{144}Nd	0.513215	Hofmann (2014)
^{176}Lu/^{177}Hf	0.038	Griffin et al. (2000)
^{176}Hf/^{177}Hf	0.283251	Griffin et al. (2000)

Natural relative abundances used to convert elemental ratios into parent/daughter ratios. CHUR compositions used as BSE estimates for ε calculations. DM compositions used for model age calculations.

The existence of large-scale variations in the Hf-Nd isotope systematics of MORB is reminiscent of the regional differences between the Indian and the Atlantic and Pacific ocean basins (Fig. 4b), initially ascribed to variable distributions of EM components based on Sr-Nd-Pb isotopes (*e.g.*Salters and Hart, 1991; Salters and White, 1998; Pearce et al., 1999). These large-scale heterogeneities, such as the so-called DUPAL anomaly (Dupré and Allègre, 1983) or the South Pacific isotopic and thermal anomaly (SOPITA; Staudigel et al., 1991), are variously regarded as consequences of plume contamination (Storey et al., 1989; Salters et al., 2011), dispersal of continental material after rifting (Arndt and Goldstein, 1989; Hanan et al., 2004; Blichert-Toft et al., 2005; Janney et al., 2005) or ancient subduction signatures (Salters and Hart, 1991; Hanan et al., 2004). Nonetheless, the existence of old and isotopically depleted domains in the convective mantle is increasingly accepted (Bizimis et al., 2007; Stracke et al., 2011; Rampone and Hofmann, 2012; Byerly and Lassiter, 2014; Sanfilippo et al., 2019; Stracke et al., 2019; Tilhac et al., 2020; Sanfilippo et al., 2021). In the emergence of this paradigm, Hf-isotope data have (1) driven a shift from a view in which recycled enriched components are the main driver of isotopic variability in oceanic lavas and (2) highlighted the fact that most oceanic lavas are isotopically more depleted than the BSE and must be dominated by depleted components.

3.3.2. *The peridotite perspective*

The first Hf-isotope analyses of peridotite were performed by Salters and Zindler (1995), overcoming the low Hf concentrations by using a secondary-ion mass spectrometry (hot SIMS) technique (Salters, 1994). The pioneering application of the Lu-Hf system to Salt Lake Crater (SLC) xenoliths from Hawaii revealed that sub-oceanic mantle peridotites could exhibit extremely radiogenic Hf-isotope compositions (ε_{Hf} up to +76) far exceeding those of basalts (Salters and Zindler, 1995). This observation suggested that the isotopic variability of MORB reflects the contribution of such peridotites with radiogenic Hf and thus that the Lu-Hf isotope system could constrain the origin of HFSE-depleted material (Salters and Shimizu, 1988; Salters and Zindler, 1995). Accordingly, most subsequent peridotite studies (Rampone and Hofmann, 2012, and

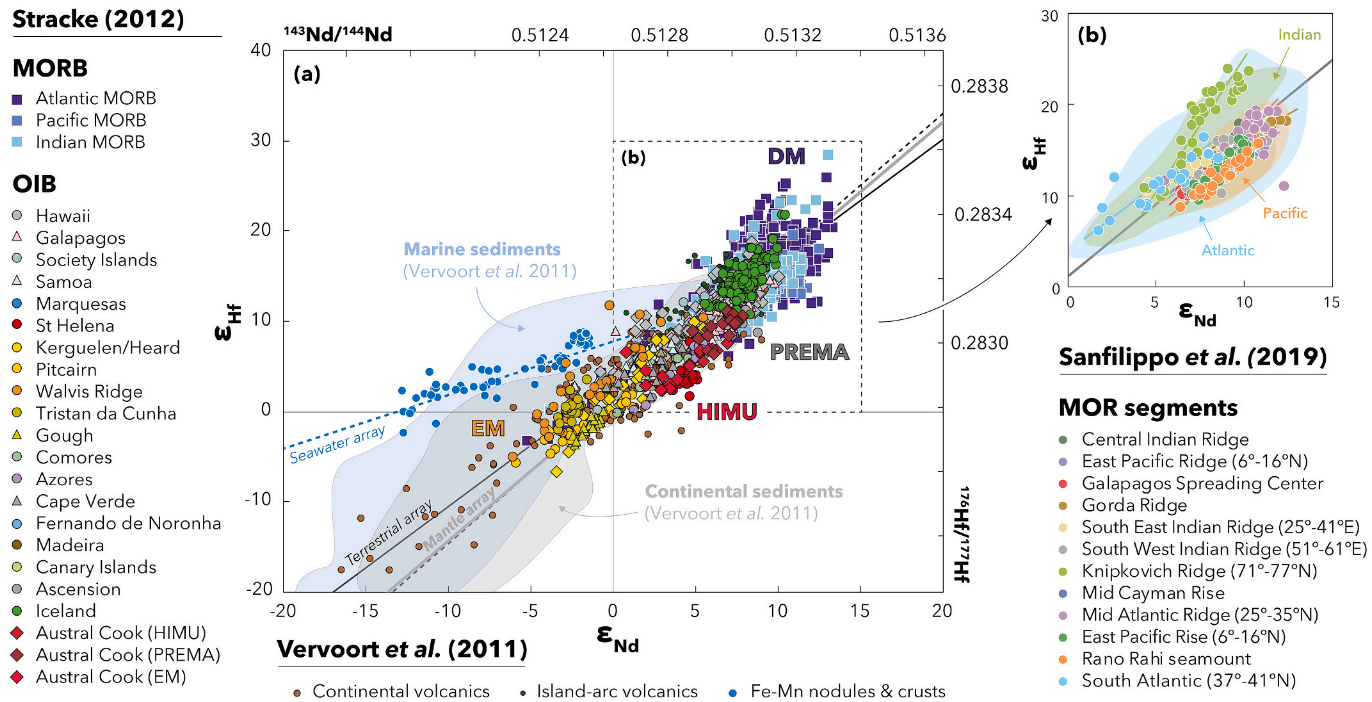

Fig. 4. (a) Plot of present-day ε_{Hf} *vs* ε_{Nd} for mid-ocean ridge (MORB) and ocean-island (OIB) basalts compiled by Stracke (2012) compared to continental and island-arc volcanics and sediments compiled by Vervoort et al. (2011). The main end-member components (DM, EM and HIMU) identified from basalt studies and discussed in the text are also shown; note that EM1 and EM2 are not well discriminated in ε_{Nd}-ε_{Hf} space. The terrestrial array of Vervoort et al. (1999) and that updated (dashed line) by Vervoort et al. (2011) are essentially identical to the mantle array of Chauvel et al. (2008). See Table 3 for more details on the different Hf-Nd arrays. (b) Correlations of individual mid-ocean ridge (MOR) segments in ε_{Nd}-ε_{Hf} space. Data compiled by Salters et al. (2011), modified after Sanfilippo et al. (2019). The Atlantic, Pacific and Indian MORB domain based on Stracke (2012)'s compilation are shown for comparison.

references therein) have tried to address two main questions:

(1) Do depleted materials represent old domains recycled/preserved in the convective mantle or more recent continental incorporation?
(2) What is their contribution to magmatic processes and volcanism?

We illustrate below some lines of reasoning developed to answer these questions through the application of Hf-Nd isotopes to the study of oceanic magmatism.

The extent to which basalt genesis takes place in melt-residue equilibrium has long been debated, notably based on the relationships between MORB and AP, which are recorded differently by different isotopic systems (Snow et al., 1994; Salters and Dick, 2002; Cipriani et al., 2004; Alard et al., 2005). Recent studies have shown that AP have significantly more radiogenic Hf (and to a lesser extent Nd) than MORB (Fig. 5), which constitutes the *AP-MORB offset* (Liu and Liang, 2017), previously observed in Os isotopes (Brandon et al., 2000; Alard et al., 2005). In the South West Indian Ridge (SWIR), the Hf-Nd isotope compositions of AP exceed those of associated SWIR basalts (Mallick et al., 2015; Frisby et al., 2016a). In the ultraslow-spreading Gakkel ridge in the Arctic Ocean, the Hf-Nd depletion recorded in AP extends the Hf-Nd mantle array to $\varepsilon_{Hf} = +60$ and $\varepsilon_{Nd} = +20$ and reaches up to $\varepsilon_{Hf} = +104$ (Stracke et al., 2011). However, these observations as well as Os-isotope data (Liu et al., 2008; Liu et al., 2022) have mostly been interpreted in terms of the presence of ultra-depleted domains in the asthenosphere. To account for the AP-MORB offset, Byerly and Lassiter (2014) postulated that either AP preferentially sample volumetrically minor, low-density, isotopically depleted domains (*i.e.* "slag" hypothesis) or that these domains are too refractory to significantly contribute to MORB genesis (*i.e.* "ghost" hypothesis) – see also Liu et al. (2020). Alternatively, enriched and depleted components may coexist but MORB are dominated by the enriched components (*i.e.* "hybrid" hypothesis) owing to the preferential melting of fertile peridotites or pyroxenites (Byerly and Lassiter, 2014). For instance, the Nd- and Hf-isotope compositions of SWIR basalts preserve both depleted and enriched signatures while the latter are not observed in the collocated peridotites (Mallick et al., 2015).

Lastly, such considerations challenge the concept of DM as the MORB source, or depleted MORB mantle (DMM). Oceanic basalts underestimate the heterogeneity of their source and particularly the abundance of depleted lithologies and/or their extent of depletion (Stracke, 2021, and references therein): 5% of an enriched component can account for ~40% of the Hf and Nd budget in the SWIR basalts (Mallick et al., 2015). Depleted-mantle models based on global MORB compositions have REE concentrations 5–40% higher (Salters and Stracke, 2004) than those of abyssal peridotites (Workman and Hart, 2005); Carlson and Ionov (2019) estimated a more fertile composition based on a set of Mongolian lherzolite xenoliths. Representativity is a major issue in the task of determining "average" mantle compositions and imparts significant uncertainties for mass balance and the timescales of early-Earth differentiation models because the volumetric characterization of the DM depends on its estimated degree of depletion (Stracke et al., 2011 and references therein).

4. Decoupling of Hf and Nd isotopes

To further understand the records of ancient depletion in the sub-oceanic mantle, we now review the main mechanisms responsible for the decoupling of Hf and Nd isotopes. Hafnium-Nd decoupling is implied when a data point plots off the mantle array in ε_{Nd}-ε_{Hf} space. Following Johnson and Beard (1993), it is measured by the $\Delta\varepsilon_{Hf}$ notation as the vertical shift between this data point and the mantle array (Fig. 6): for instance, $\Delta\varepsilon_{Hf} = \varepsilon_{Hf} - (1.59 \times \varepsilon_{Nd} + 1.28)$ using the array of Chauvel et al. (2008). For simplicity, we will use *negative decoupling* to refer to points lying below the mantle array (*i.e.* yielding negative $\Delta\varepsilon_{Hf}$), and *positive decoupling* to refer to those above the array (positive $\Delta\varepsilon_{Hf}$), which

Table 3
Mantle, terrestrial, sediment and other Hf-Nd arrays.

Array	Slope	Intercept	Reference	Comment
Mantle	1.59	1.28	Chauvel et al. (2008)	MORB & OIB
Terrestrial (new)	1.55	1.21	Vervoort et al. (2011)	Including new marine sediment data
Terrestrial	1.36	2.95	Vervoort et al. (1999)	Mantle & crustal samples
Crustal	1.35	2.82	Vervoort et al. (1999)	Sediments, continental basalts, granitoids & juvenile crustal rocks
All ocean basalts	1.33	3.19	Vervoort et al. (1999)	MORB, OIB & island-arc volcanics
Ocean-island basalts	1.51	1.39	Chauvel et al. (2008)	
Ocean-island basalts	1.42	2.57	Vervoort et al. (1999)	
Ocean-island basalts	1.36	1.63	Johnson and Beard (1993)	
Island arcs	1.23	6.36	Chauvel et al. (2009)	
Island-arc volcanics	1.27	4.87	Vervoort et al. (1999)	
Clays	0.78	5.23	Bayon et al. (2016)	
Dust clays	0.45	2.85	Zhao et al. (2014)	Mongolian & Chinese dust clays
Muds	1.44	3.48	Vervoort et al. (1999)	
Sands	1.84	1.98	Vervoort et al. (1999)	
Recycled orogenic sands	1.83	0.60	Vervoort et al. (1999)	
All sediments	1.67	2.82	Vervoort et al. (1999)	
Sediments	1.45	3.19	Vervoort et al. (1999)	Excluding recycled orogenic sands
Zircon-free sediments	0.91	3.10	Bayon et al. (2009)	
Zircon-bearing	1.80	2.35	Bayon et al. (2009)	
Seawater	0.55	7.10	Albarède et al. (1998)	Fe-Mn crusts & nodules
Juvenile whole rocks	1.40	2.10	Vervoort and Blichert-Toft (1999)	Excluding early Archean WR gneisses from West Greenland
All whole rocks	1.36	3.00	Vervoort and Blichert-Toft (1999)	Juvenile, early Archean & other WR data
Apollo 12 basalts	3.80	7.00	Vervoort et al. (1999)	

MORB, mid-ocean ridge basalts; OIB, ocean-island basalts; IAV, island-arc volcanics; WR, whole rock. Intercepts are given as published (*i.e.* based on the BSE estimates available at the time); the mantle array is within error of the most recent BSE estimates (Bouvier et al., 2008). Note that inverse linear correlations are observed between intercept and slope for all arrays except that of Apollo 12 basalts (Electronic Appendix Fig. A2).

by far is the more common situation; 40% of the compiled data have $\Delta\varepsilon_{Hf} > 10$ (Fig. 7). This proportion is similar in peridotites and pyroxenites, showing that (decoupled) depleted isotopic signatures are not carried only by refractory lithologies.

4.1. Positive decoupling (above the mantle array)

Studies of the SLC peridotite xenoliths from Hawaii provided the basic conceptual framework to explain positive Hf-Nd decoupling (Salters and Zindler, 1995; Bizimis et al., 2003; Bizimis et al., 2005). Decoupling has been increasingly reported in xenoliths from various continental environments, both on-craton (Schmidberger et al., 2002; Bedini et al., 2004; Carlson et al., 2004; Wittig et al., 2006) and off-craton (Ionov et al., 2005b), in orogenic massifs (Pearson and Nowell, 2004; Le Roux et al., 2009; Tilhac et al., 2020) and in abyssal peridotites (Stracke et al., 2011). This has led to the emergence of many similar models, mostly involving ancient depletion and metasomatic overprint; two main kinds are distinguished below (Fig. 6a). These exclude the preferential mobilization of Nd (lowering Sm/Nd) during serpentinization and seawater alteration (Frisby et al., 2016a) which is mainly relevant to abyssal peridotites and the sources of arc volcanism.

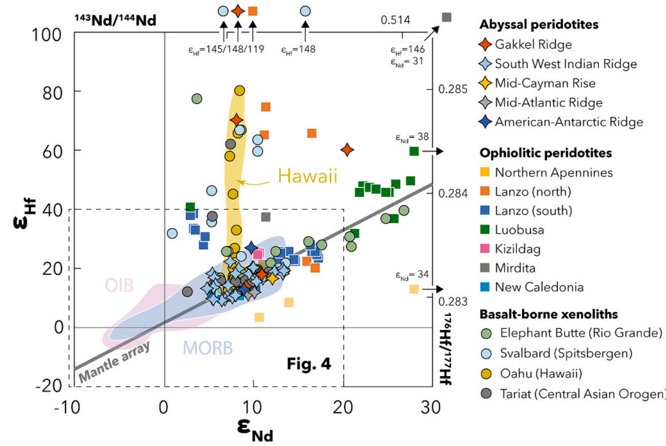

Fig. 5. Plot of present-day ε_{Hf} *vs* ε_{Nd} for abyssal and ophiolitic peridotites. The compositional fields of MORB and OIB (as detailed in Fig. 4), and selected localities of basalt-borne xenoliths relevant to the discussion are shown for comparison. Source references are listed in Tables 1a and 1b.

4.1.1. Fractionation models

Fractionation models are essentially single-stage models where differential fractionation of Lu/Hf with respect to Sm/Nd occurs during partial melting, particularly in the presence of garnet (Schmidberger et al., 2002), or sub-solidus transition between spinel and garnet (Ionov et al., 2005b; Zhang et al., 2012), and is followed by radiogenic ingrowth. Garnet strongly retains Lu and fractionates Lu/Hf, leading in time to positive decoupling in the residues, proportionally to the degree of melting and age. As illustrated in Fig. 6b, these models are quite dependent on the choice of melting reaction and partition coefficients. They are commonly used to explain samples that are scattered at high ε_{Nd} and extend the mantle array beyond the DM (Fig. 5), such as the coupled Hf-Nd depletion observed in some Gakkel ridge AP (Stracke et al., 2011) or in peridotites from the Itsaq Gneiss Complex in Greenland (van de Löcht et al., 2020), among other examples (*e.g.* Shaw et al., 2007; Bianchini et al., 2014; Byerly and Lassiter, 2014).

4.1.2. Mixing models

Mixing models are two-stage models in which Nd isotopes are preferentially reset from a depleted component whose radiogenic Hf is at least partly preserved (Bizimis et al., 2003; Wittig et al., 2007; Yu et al., 2009; Stracke et al., 2011). They are used for samples characterized by relatively unradiogenic Nd (*e.g* comparable to oceanic basalts) and a near-vertical spread in ε_{Nd}-ε_{Hf} space potentially reaching extremely radiogenic Hf (Fig. 2a). These models all require ancient and/or high degrees of melting to generate the radiogenic component and mostly differ in the mechanism that preferentially re-equilibrates Nd isotopes: simple mixing, assimilation-fractionation crystallization (AFC) or more complex formulations. In a simple mixing situation (*i.e.* 0D), positive decoupling occurs if the radiogenic component has a sufficiently high Hf/Nd (compared to the unradiogenic component) to produce concave-downward trends in ε_{Nd}-ε_{Hf} space (Fig. 6b). In a percolation situation (*i.e.* 1D), positive decoupling may occur in the percolated protolith *via* chromatographic re-equilibration if Nd re-equilibrates more readily than Hf (*i.e.* $Kd^{Hf} > Kd^{Nd}$), provided that porosity (*i.e.* melt proportion) is low and grain size is small. Such decoupling is transient and increases

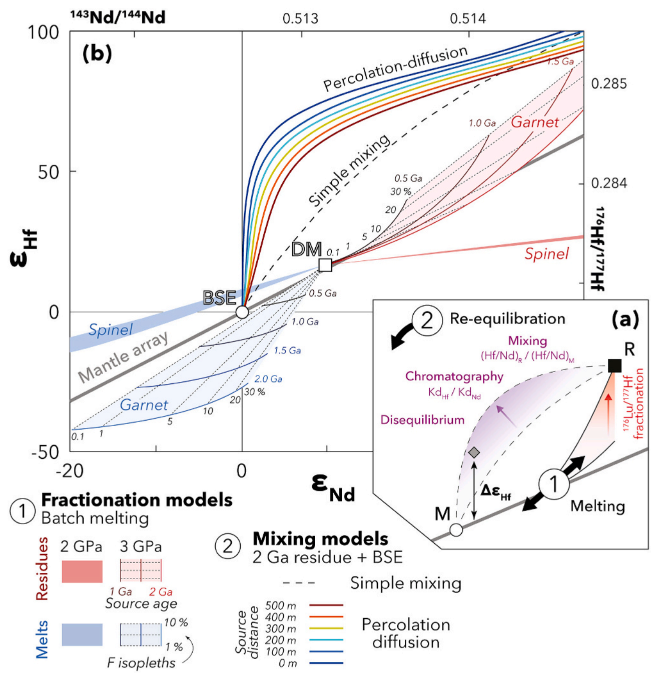

Fig. 6. (a) Summary of the main mechanisms accounting for the decoupling and re-coupling of Hf and Nd isotopes in ε_{Nd}-ε_{Hf} space. A decoupled data point (grey diamond) is shown as an example of $\Delta\varepsilon_{Hf}$ calculation. Positive decoupling can occur (1) following radiogenic ingrowth as a result of preferential fractionation of Lu/Hf during partial melting (in red) or (2) during partial re-equilibration (*e.g.* mixing, melt-periodite interaction, AFC, *etc.*) between a radiogenic residue (R) and an unradiogenic melt (M); the opposite situation is also considered in the text but remains conceptually the same: the radiogenic component must have a higher Hf/Nd ratio than the unradiogenic component (in purple). In a melt-percolation situation, preferential partitioning of Nd into the melt and chemical disequilibrium may also promote stronger decoupling. The re-equilibration process may eventually lead to re-coupling to the mantle array. (b) Examples of models simulating Hf-Nd decoupling mechanisms. In (1) are shown, as an example of fractionation (*i.e.* single-stage) models, the compositions of melts (in blue) and residues (in red) obtained from batch melting models at different melting degrees (0.1–30%) after various extents of radiogenic ingrowth (0.5–2.0 Ga). Two situations are considered: melting in the spinel- (2 GPa) and garnet- (3 GPa) stability fields. In detail, the melting models are calculated from the DM whose isotopic compositions is first back-calculated at the age indicated; an equivalent time is then used to calculate radiogenic ingrowth in the modelled melts and residues. Partition and melting coefficients as well as modal compositions at 2 and 3 GPa are taken from Salters and Stracke (2004); the source composition is taken from Workman and Hart (2005). In (2) are shown, as an example of mixing (*i.e.* two-stage) models, the solid compositions obtained from a simple mixing between a radiogenic component taken as a 2-Gy old melting residue obtained in (1) and the Bulk Silicate Earth (BSE), which lies within the array of oceanic basalts. A percolation-diffusion model shows the reaction between these same two components in the form of a residual peridotitic protolith percolated (porous flow) by a basaltic melt. In this model, modified from Tilhac et al. (2020), the solid matrix is represented by 0.1-mm cpx spheres where melt percolation occurs in 1% porosity. The trace-element composition of the melt considered is comparable to an arc melt (*i.e.* with relatively low Hf/Nd). Rainbow colours indicate the position of the solid within the percolated column (>0 to 500 m from the bottom). Variations observed at different positions reflect the effects of chromatographic fractionation. In the situation shown here where $Kd^{Hf} < Kd^{Nd}$, chromatography lessens the extent of decoupling (*i.e.* decreasing from blue to red), which suggests that positive decoupling is expected from such melt-rock interaction scenario regardless of the partition coefficients considered. In the opposite and certainly more common situation where $Kd^{Hf} > Kd^{Nd}$, chromatography would produce even stronger decoupling, as illustrated in (a). See Tilhac et al. (2020) for more detail on the percolation-diffusion model parameters.

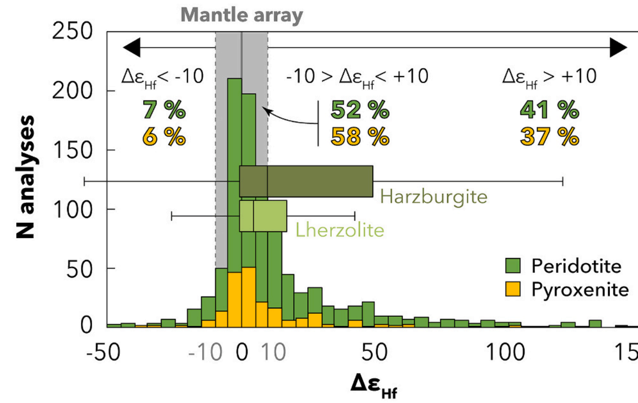

Fig. 7. Histogram of present-day $\Delta\varepsilon_{Hf}$ showing the extent of Hf-Nd isotope decoupling in peridotites and pyroxenites from the global dataset. Percentages show the proportion of these rocks that have $\Delta\varepsilon_{Hf}<-10$ (negatively decoupled), $-10<\Delta\varepsilon_{Hf}<+10$ (coupled) and $> +10$ (positively decoupled), respectively, which is similar in peridotites and pyroxenites. The difference between lherzolites and harzburgites is shown in a box-and-whisker plot for comparison.

away from the melt source until the percolated protolith is fully re-equilibrated and its Hf-Nd isotopes are "re-coupled" (Fig. 6b).

Based on the ancient melt depletion (AMD) and mantle-melt interaction (MMI) models of Salters and Zindler (1995), the radiogenic component may be either a peridotitic melt residue (*i.e.* AMD) or a melt (*i.e.* MMI). The former case requires ancient melting, which can be recorded by old Os signatures (Bizimis et al., 2007; Tilhac et al., 2020), and recent re-enrichment (Bizimis et al., 2005; Wittig et al., 2007; Stracke et al., 2011; Tilhac et al., 2020), often resulting in future model ages (Salters and Zindler, 1995; Aulbach et al., 2004; Yu et al., 2009; Choi and Mukasa, 2012). The trace-element systematics and Nd-isotope compositions of the mixing product reflect the metasomatic agent whereas Hf isotopes reflect the residual protolith. Alternatively, the radiogenic component can be carried by the metasomatic agent (Bizimis et al., 2003; Sanfilippo et al., 2019). This mechanism is supported by the REE depletion and Hf-Nd decoupling observed in the replacive harzburgite bodies from the Lanzo massif, which contrasts with the MORB-like signature of their host plagioclase peridotites (Sanfilippo et al., 2019). The melt can acquire a depleted signature with high Lu/Hf through interaction with residual peridotites such as stratified lithospheric residues or AFC-like processes (Salters and Zindler, 1995; Bizimis et al., 2003), which potentially occur during plume-lithosphere interaction. However, these depleted melts are never directly observed, perhaps because their strong incompatible-element depletion make their signature easily "diluted" (Sanfilippo et al., 2019).

4.1.3. Chemical disequilibrium

To account for positive decoupling, most mixing models rely on the time integration of depletion and enrichment events and on the relative mobility of Nd with respect to Hf. However, decoupling of these two isotope systems may also represent a kinetic effect associated with solid-liquid disequilibrium during melt transport (Le Roux et al., 2009; Tilhac et al., 2020). Percolation-diffusion models show that slow re-equilibration due to the low diffusivities of Hf (Bloch and Ganguly, 2014), and to a lesser extent Nd (Van Orman et al., 2001), inhibits the chromatographic effect. As a consequence, melt percolation systematically induces a positive Hf-Nd decoupling in the percolated solid (Tilhac et al., 2020), essentially regardless of the partition coefficients used, even if $Kd^{Hf} < Kd^{Nd}$ (Fig. 6b).

Under conditions where diffusional disequilibrium prevails, the relative chemical diffusivities and the efficiency of isotopic homogenization control the Hf and Nd budgets at any given point in time and space (Le Roux et al., 2009). Nonetheless, the starting compositions of the melt and protolith also matter, as described for the simple mixing situation (Fig. 6a). Tilhac et al. (2020) emphasized that HFSE-depleted melts such as arc magmas provide an unradiogenic component with low Hf/Nd promoting positive Hf-Nd decoupling and invoked a picritic/bonitic melt to explain $\Delta\varepsilon_{Hf}$ up to +140 in the pyroxenites from the Cabo Ortegal Complex, NW Spain. The importance of the Hf/Nd in the percolating melt can also be illustrated by xenoliths from the northern Massif Central with decoupled ε_{Hf} up to +2600 ascribed to hydrous/carbonatitic, low-HFSE metasomatism. In contrast, coupling (or indeed, "re-coupling") of Nd and Hf isotopes in the southern Massif Central was ascribed to silicate metasomatism and the dichotomy linked to regional variations in lithospheric thickness controlling the melt compositions (Wittig et al., 2007).

We conclude that, with some exceptions, positively decoupled Hf-Nd isotopes reflect partial re-equilibration during (transient) melt-peridotite interaction processes whereas their (re)-coupling documents more advanced stages of re-equilibration (*e.g.* Choi and Mukasa, 2012; Sanfilippo et al., 2022). However, while decoupling clearly hints at the involvement of ancient, depleted material, coupling does not rule out this possibility. On the contrary, many localities exhibit a vertical scattering in ε_{Nd}-ε_{Hf} space (*e.g.* SLC peridotites) which suggests that the maximum ε_{Hf} underestimates that of the original protolith (and thus its age and/or depletion). This interpretation is consistent with the systematic decoupling of most data points with extremely radiogenic Hf (*e.g.* Fig. 2) and with the range of $\Delta\varepsilon_{Hf}$ in harzburgites globally exceeding that of lherzolites (Fig. 7), which are often interpreted as products of refertilization (Le Roux et al., 2007).

4.2. Negative decoupling (below the mantle array)

Decoupling below the mantle array is less common (<6–7% of the dataset; Fig. 7), often observed in garnet pyroxenites and eclogites, and always restricted to low $|\Delta\varepsilon_{Hf}|$ values. This decoupling is typically ascribed to the recycling of oceanic crust (Pearson and Nowell, 2004; Wu et al., 2006; Doucet et al., 2015; Varas-Reus et al., 2018; Fitzpayne et al., 2019; Ackerman et al., 2020), because it is consistent with the long-term preservation of melt compositions with low Lu/Hf relative to Sm/Nd (*i.e.* in blue in Fig. 6b), such as MORB and oceanic gabbros (Chauvel et al., 2008). This process (accompanied or not by sediment recycling) is often the preferred scenario for HIMU basalts provided that substantial changes in P/D ratios (especially for Pb isotopes) occur during subduction metamorphism (Stracke et al., 2003, and references therein). For instance, recycled protoliths including oceanic sediments and gabbros were proposed for the Bohemian Massif pyroxenites whose range in initial ε_{Hf} (−6.4 to +66) also suggests the involvement of a depleted component documented by unradiogenic initial Os (Ackerman et al., 2016). However, the isotopic heterogeneity of SCLM-derived mafic lithologies such as pyroxenites and eclogites ascribed to crustal recycling processes (Gonzaga et al., 2010) contrasts with the remarkable isotopic uniformity of HIMU basalts (Stracke et al., 2005; Stracke, 2012). This apparent contradiction may indicate that mafic lithologies with HIMU-like signatures reflect slab-derived metasomatic components stored at sub-lithospheric levels and activated during rifting (*e.g.* Beccaluva et al., 2011; Bianchini et al., 2014) rather than an origin as recycled slab material.

5. Geodynamic perspectives from the SCLM

5.1. Origin and evolution of the SCLM

Many studies of cratonic xenoliths from the Kaapvaal, Canadian and Sino-Korean cratons (Aulbach et al., 2004; Bedini et al., 2004; Carlson et al., 2004; Wu et al., 2006; Choi and Mukasa, 2012; Liu et al., 2012; Shu et al., 2014) have been primarily concerned with the thermal history of the continental lithosphere – see Pearson et al. (2014). Lutetium-Hf isochron ages coupled with Re-Os systematics in WR samples (Wu et al., 2006) and sulfides (Aulbach et al., 2004) have provided constraints on the timing of melt extraction marking stabilization of the SCLM (*e.g.* Choi and Mukasa, 2012). Some studies have also addressed in detail the validity of concepts such as isotopic equilibrium and blocking temperatures in order to precisely establish geothermal gradients and cooling rates (*e.g.* Bedini et al., 2004; Lazarov et al., 2012a; Shu et al., 2014). However, deconvoluting age from mixing relationships in radiogenic-isotope data remains an issue (Electronic Appendix 3) bearing on the spatio-temporal characterization of the SCLM, as illustrated below.

5.1.1. Origin and assembly of the cratonic lithosphere

Current views on the dominant style of tectonics in the Archean vary between two end members: plate (*i.e.* horizontal) *versus* non-plate (*i.e.* vertical) tectonics (*e.g.* Van Kranendonk et al., 2007). In the Kaapvaal Craton, the origin of the residual SCLM and its unusually high SiO_2 (hence opx) contents has been attributed to both a "plume" model where melting occurred in the garnet stability field and a "ridge" model where melting in the spinel stability field was followed by subduction-related enrichment (Shu et al., 2013, and references therein). The debate often hinges on the interpretation of age constraints and their relationships to crustal magmatic/tectonic episodes and the assembly history of the craton (*e.g.* Simon et al., 2007; Begg et al., 2009; Shu et al., 2013). Such constraints are notably provided by Hf-Nd isotope studies of kimberlite-borne xenoliths and subcalcic garnet xenocrysts from cpx-free harzburgites and dunites (Lazarov et al., 2009; Shu et al., 2013; Shu and Brey, 2015). Near the major suture of the Kaapvaal Craton (Colesberg Lineament; see Fig. 1 in Shu and Brey, 2015), the abundance of eclogite xenoliths in Roberts Victor kimberlite has been proposed as evidence for the former existence and subduction of oceanic lithosphere (Gonzaga et al., 2010). Roberts Victor garnets indeed yield a Lu-Hf isochron at 2.9 Ga coincident with the inferred time of amalgamation of the east and west blocks (Schmitz et al., 2004) and their low initial ε_{Hf} (+2.7) specifies a PM-like protolith which is compatible with an oceanic setting (Shu et al., 2013). However, the oceanic origin of Roberts Victor eclogites has been strongly questioned (Huang et al., 2012; Gréau et al., 2013; Huang et al., 2022). In contrast, subcalcic garnets from Finsch peridotites yield a 2.6 Ga isochron whose high initial ε_{Hf} (+26) argues in favour of ancient metasomatism of a depleted protolith (Shu et al., 2013), potentially dated by sulfide T_{RD} ages at 3.2 Ga (Griffin et al., 2004).

Data from the western Kaapvaal Craton (mostly garnets from Finsch but also from Roberts Victor, Bellsbank and Bulfontein kimberlites) vary widely, mostly towards high present-day ε_{Hf} and low ε_{Nd} (Fig. 8a); many data points reach several hundreds and even thousands of ε_{Hf} units, up to ε_{Hf} = +13,753, the highest of the whole dataset (Fig. 2a). This characteristic decoupling towards negative ε_{Nd} and positive ε_{Hf} has been taken as evidence for the overprint of a HREE-depleted protolith by a low Hf/Nd melt derived from a source with very low Sm/Nd (Simon et al., 2007; Shu and Brey, 2015). Small degrees of such metasomatism could leave Hf isotopes little affected, resulting in an evolution towards low ε_{Nd} at nearly constant ε_{Hf} (*i.e.* positive decoupling) whereas higher degrees overwhelmed the Hf signature of the protolith, bringing the affected samples below the mantle array (*i.e.* negative decoupling). Ancient interaction with a carbonatitic melt is often preferred to account for this signature (Fig. 8b), but recent contamination by kimberlite has also been invoked, for instance in the group-I, Cretaceous xenoliths of Simon et al. (2007), highlighting the difficulty of distinguishing ancient from recent overprints (Shu and Brey, 2015).

In the Canadian Arctic, the study of the Nikos kimberlite on Somerset Island (Schmidberger et al., 2002) – the first Hf-isotope data ever reported for kimberlite-borne xenoliths – is also relevant to the spatial variability and assembly history of the cratonic lithosphere. Low-temperature (<1100 °C) peridotites exhibit markedly decoupled Hf-Nd isotopes with ε_{Hf} up to ∼ + 100, whereas peridotites equilibrated at higher temperatures plot near the mantle array (Fig. 8b). This observation was interpreted as reflecting the vertical stratification of the

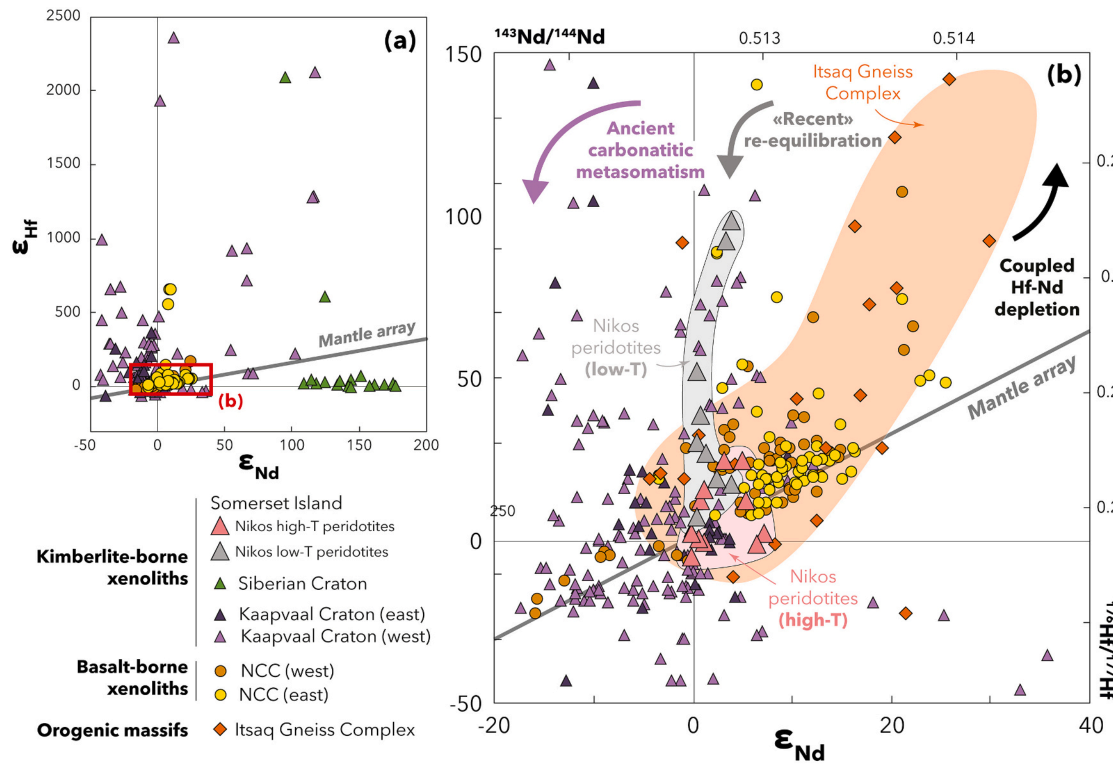

Fig. 8. Plot of present-day ε_{Hf} *vs* ε_{Nd} for selected localities of cratonic SCLM including kimberlite- and basalt-borne xenoliths and orogenic massifs. The full extent of their isotopic variability is shown in (a); note that the xenoliths from Udachnaya kimberlites in the Siberian Craton plot significantly below the mantle array. The ε_{Nd}-ε_{Hf} space is restricted to ε_{Hf} − 50 to +150 and ε_{Nd} − 20 to +40 in (b) to show the different processes (arrows) discussed in *Section 5.2*. The re-coupling of Nikos low- and high-temperature peridotites discussed in the text is also shown. Source references are listed in Tables 1a and 1b.

North American Craton with a shallow lithosphere stabilized in the Archean and more recent mantle accreted at depth (Schmidberger et al., 2002). Whole-rock compositions of the low-temperature xenoliths indeed plot close to a reference isochron of 2.8 Ga equivalent to the oldest sulfide *Re*-depletion age (T_{RD}) population in the same rocks (Bragagni et al., 2017). However, these samples exhibit a positive decoupling with a vertical spread in ε_{Nd}-ε_{Hf} space (Fig. 8b) and a correlation between $^{176}Hf/^{177}Hf$ and 1/Hf (Electronic Appendix Fig. A5), suggesting that Hf was partially re-equilibrated during a mixing process that homogenized Nd isotopes to values close to that of the host kimberlites.

In the Siberian Craton, peridotite xenoliths from the Udachnaya kimberlite exhibit a wide range of ε_{Nd} (+100–175) and relatively homogeneous ε_{Hf} (<+70) mostly plotting below the mantle array (Fig. 8a). The distribution of Udachnaya peridotites in present-day ε_{Nd}-ε_{Hf} space, unique in the whole dataset, has two exceptions with coupled Hf-Nd depletion reaching extremely high ε_{Hf} that plot above the array. These samples define a 1.8-Ga Lu-Hf isochron, interpreted as related to a major melting episode accompanying the stabilization of the central Siberian craton (Doucet et al., 2015), whereas the formation age of many other cratons is *ca* 2.7. Doucet et al. (2015) proposed that this peculiar age, which coincides with an episode of crustal generation globally documented by U-Pb ages from detrital zircons and by T_{RD} ages in the Slave and North Atlantic cratons, represents the latest formation of cratonic lithosphere and a transition from Archean to modern tectonics. However, although the Lu-Hf isochron is consistent with model ages (Electronic Appendix 3), its initial ε_{Hf} of −34 is not compatible with pristine melting residues from a PM-like protolith. From a Hf-Nd perspective (and the Os-isotope sulfide data), it is more likely that Udachnaya peridotites represent Archean protoliths (*e.g.*Pearson et al., 1995; Griffin et al., 2002; Tretiakova et al., 2017) variously overprinted by a tectono-thermal event at 1.8–1.9 Ga (Koreshkova et al., 2009, and references therein), corresponding to the collisional peak of the Columbia supercontinent (Zhao et al., 2002; Zhao et al., 2004) and thus to plate-tectonic processes. The locality is accordingly classified as a reworked Archean (P/A) terrane (Tables 1a and 1b).

In contrast to the examples above, the ultramafic bodies of the Itsaq Gneiss Complex in SW Greenland are characterized by strikingly coupled Hf-Nd depletion extending towards very radiogenic values (Fig. 8b) and consistent Sm-Nd and Lu-Hf isochron ages at 3.8–3.9 Ga yielding depleted initial ε_{Nd} and ε_{Hf} of +3–4. These samples are the only Archean ultramafic suite preserving such a coupled Hf-Nd depletion. They are interpreted as hydrous melting residues overprinted by TTG−/adakite-like metasomatism hinting at Eoarchean subduction processes (van de Löcht et al., 2020).

5.1.2. *Destruction of ancient lithosphere*

The extent of preservation *vs* destruction of the cratonic lithosphere and the role of mantle metasomatism are recurring issues in the SCLM literature. In many peridotite occurrences in reworked Archean terranes, ancient melt-depletion events are identified by old *Re*-Os and Lu-Hf ages (Schmidberger et al., 2002; Pearson and Nowell, 2004; Lapen et al., 2005; Wittig et al., 2006, 2007; Choi et al., 2010). However, their interpretations often face a “chicken and the egg” dilemma: is the ancient signature preserved from an original protolith in the lithosphere or was it introduced by melts themselves derived from ancient material present in the convective mantle? Geochronological data alone usually cannot distinguish between these alternatives, especially since mixing/isochron relationships often are also ambiguous (Electronic Appendix 3). This issue underpins debates on the assembly history of the NCC (Liu et al., 2012; Zhao et al., 2021) and the origin of Proterozoic melt-depletion ages in peridotite xenoliths from the eastern NCC (Chu et al., 2009, and references therein), among other of such examples in eastern China (*e.g.*Liu et al., 2017b), western and central Europe, eastern Australia or the western USA (Pearson et al., 2014, and references therein). We propose that positive Hf-Nd decoupling could generally be taken as a proxy for lithospheric melt-peridotite interaction involving ancient protoliths.

The presence of Ordovician diamondiferous kimberlites in the NCC indicates the existence, at least locally, of a thick lithosphere in the Palaeozoic, but geophysical observations and abundant mantle peridotites hosted by Cenozoic alkali basalts indicate that the lithosphere is now thinner and hotter (Sun et al., 2021, for a review). This provides two incomplete but complementary snapshots of the evolution of the cratonic lithosphere (Griffin et al., 1998; Wu et al., 2006; Chu et al., 2009; Yang et al., 2010). However, the nature of the process by which Mesozoic lithospheric thinning occurred is strongly debated (*e.g.* Wu et al., 2006, and references therein). On the one hand, delamination has been postulated based on the compositions of large volumes of Mesozoic igneous rocks compatible with the presence of ancient mafic crust in their source (Gao et al., 1998; Gao et al., 2004; Chu et al., 2009). The involvement of delaminated lower crust in the source of metasomatizing silicate melts was also proposed for Yangyuan basalt xenoliths (Yang et al., 2018). Similarly, mantle-array-like Hf-Nd isotopes (Fig. 8b) with Proterozoic Lu-Hf isochron ages and Os model ages in eastern NCC xenoliths from the Cenozoic Penglai and Shanwang basalts are interpreted as the record of ancient depletion events in the convective mantle (Chu et al., 2009). On the other hand, progressive "decratonization" *via* thermo-mechanical erosion is supported by Mesozoic granitoids yielding several zircon age populations since *ca* 200 Ma (Griffin et al., 1998), although debated (*e.g.* Wu et al., 2006, and references therein), and the existence of Tertiary and Holocene volcanics whose Hf-isotope compositions suggest the mixing of mantle- and crustal-derived melts (*e.g.* Yang et al., 2008). A Lu-Hf isochron at *ca* 2.5 Ga reported by Choi et al. (2008) in the "least metasomatized" xenoliths from the Hannuoba basalts also argues against complete removal of the lithospheric keel in the northern part of the NCC.

Overall, the above observations can be explained by shallow-dipping subduction caused by accelerated convergence in the mid-Jurassic to early Cretaceous and subsequent rollback of the paleo-Pacific slab (Wu et al., 2019; Sun et al., 2021). Lithospheric thinning and refertilization in eastern and southern China are indeed compatible with basal hydration weakening caused by slab dehydration and basaltic production caused by asthenospheric upwelling (Kusky et al., 2014). This scenario accounts for melt-peridotite interaction affecting ancient protoliths in the eastern NCC, as documented by xenoliths with decoupled Hf-Nd and strongly radiogenic Hf in samples with $\varepsilon_{Nd} < +15$ (Fig. 8b). It is also consistent with newly accreted, subduction-related lithosphere sampled as fertile lherzolites, for instance by the trachybasalts of Mt. Baekdu on the Chinese-North Korean border (Park et al., 2017). Accordingly, xenoliths from the western NCC localities (*e.g.* Yangyuan, Sanyitang), unaffected by the paleo-Pacific subduction, preserve cratonic SCLM as documented by coupled Hf-Nd depletion reaching ε_{Hf} values similar to the decoupled ones in the east (Fig. 8b). These considerations highlight the global importance of subduction processes during craton reactivation and the modification of ancient, refractory (initially buoyant) lithosphere (Tang et al., 2013, and references therein).

5.2. Recycling of continental material

Many Hf-Nd studies of Proterozoic (P, T/P) terranes have been used to infer the tectonic environments in which the studied lithological associations originated (*e.g.* Malaviarachchi et al., 2010). For instance, pyroxenite and hornblendite veins are often interpreted as magmatic intrusions (Choi et al., 2007; Tilhac et al., 2016; Xu et al., 2021), reflecting mantle-wedge heterogeneity (Xiong et al., 2014; Lu et al., 2018; Lu et al., 2020) and temporal changes in the subduction system (*e.g.* Siegrist et al., 2019) or alternatively, as the result of tectonic juxtaposition (Lapen et al., 2005; Bianchini et al., 2007; Zhang et al., 2020). We focus below on aspects of these studies, as well as reworked Archean terranes (T/P/A in particular), relevant to the introduction of continental material in the sub-oceanic and convective mantle.

5.2.1. Subduction-related continental recycling processes

In reworked Archean terranes, $\Delta\varepsilon_{Hf}$ tends to decrease from P/A to T/P/A and T/A (Fig. 9) and this trend is accompanied by a slight overall shift towards radiogenic Nd with correlated with the number of arc−/back-related events documented (Electronic Appendix Fig. A6). We postulate below that such a global progression from decoupled Hf-Nd and unradiogenic Nd towards array-like compositions reflects the reworking of continental material by arc magmas and/or their reprocessing in mantle-wedge environments and/or beneath mid-ocean ridges.

Compared to Proterozoic pyroxenites (Fig. 10b), "recent" pyroxenites (*i.e.* from Tecton terranes, T) strikingly overlap abyssal peridotites along the Hf-Nd mantle array (compare Fig. 5 & 10a), suggesting that these pyroxenites crystallized from melts mostly derived from the convective mantle, while T peridotites show a wide range of coupled Hf-Nd depletion (Fig. 10a). In contrast, pyroxenites from reworked Archean localities plot along, or slightly below, the mantle array over a wide range of ε_{Nd} whereas the peridotites are positively decoupled (Fig. 10c). These pyroxenite localities correspond to terranes with documented suture zones and/or arc-related history (Tables 1a and 1b). Among them, the diversity of mantle pyroxenites in the Beni Bousera and Ronda massifs reflects the recycling of variously old oceanic and continental lithospheric material (Varas-Reus et al., 2018), as documented by low ε_{Hf} and ε_{Nd} (Fig. 11a) and low $^{206}Pb/^{204}Pb$ in the group-B samples (*i.e.* with EM2-like Sr-Nd-Hf systematics), and *Re*-Os model ages and Lu-Hf isochron ages of 1.2–1.4 Ga (Pearson and Nowell, 2004 and references therein). The recycling of continental lower crust has also been suggested to explain quartz-bearing garnet clinopyroxenites from the Malaita alnoïte with EM1-like Pb and Sr isotopes and decoupled Hf-Nd isotopes (Ishikawa et al., 2007), in contrast to other xenoliths that plot near the mantle array (Fig. 11a). Subduction-related processes thus provide a mechanism for the introduction of both oceanic and

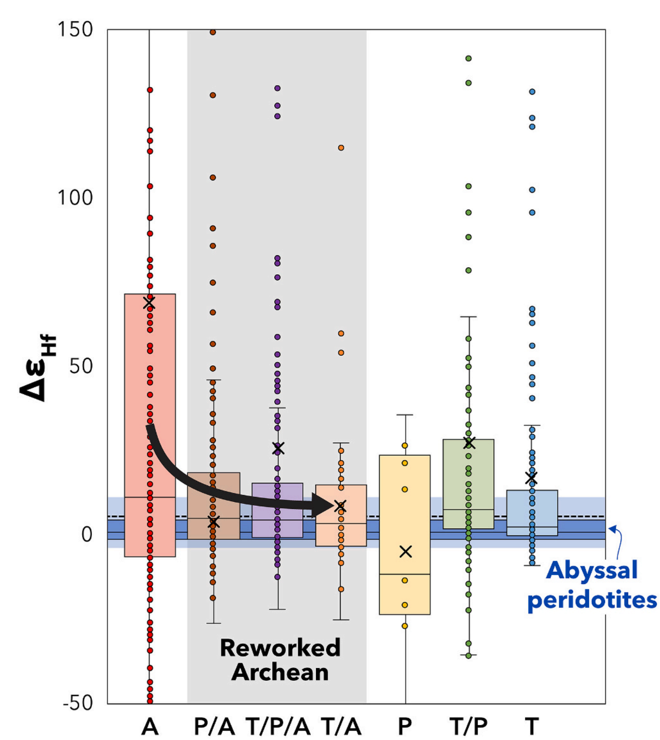

Fig. 9. Box-and-whisker plot of present-day $\Delta\varepsilon_{Hf}$ showing the extent of Hf-Nd isotopic decoupling between populations of different tectono-thermal age. Both the mean values and data range towards positively decoupled values decrease from A through P/A, T/P/A and T/A to overlap with the values observed in abyssal peridotites, shown for comparison in blue (their average value is shown by a dashed line). (For interpretation of the references to colour in this figure legend, the reader is referred to the web version of this article.)

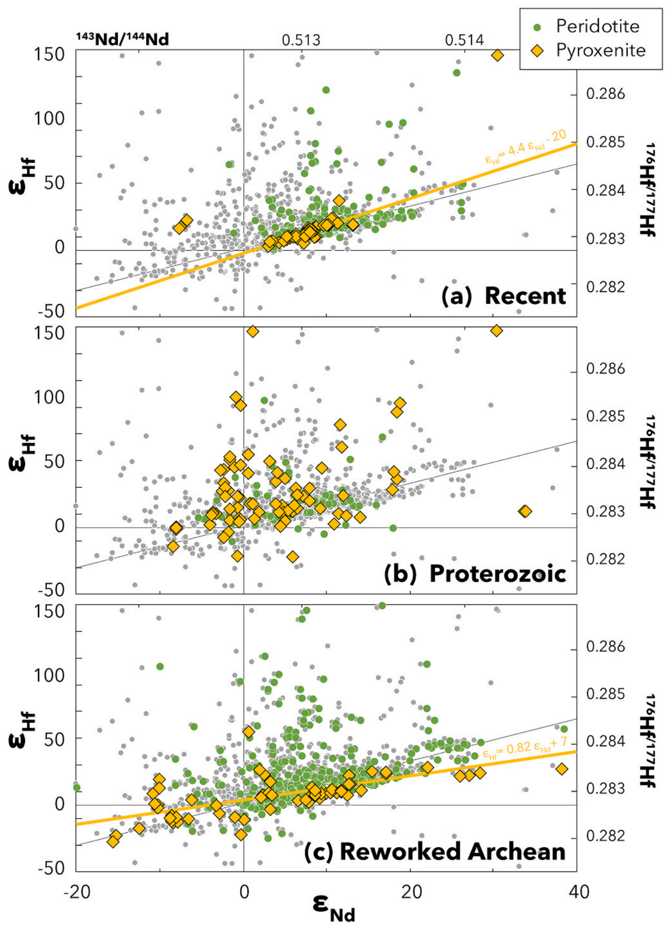

Fig. 10. Plot of present-day ε_{Hf} *vs* ε_{Nd} in peridotites and pyroxenites from recent (a), Proterozoic (b) and reworked Archean (c) terranes; *Recent* here refers to localities classified as T as well as abyssal peridotites; *Proterozoic* refers to both preserved and reworked terranes (P and T/P); *Reworked Archean* refers to P/A, T/P/A and T/A. Note the preferential distribution of reworked Archean pyroxenites near or below the mantle array (c), contrasting with their scattering in Proterozoic occurrences (b) and their restriction to basaltic (*i.e.* mantle-array-like) compositions in recent terranes (a). Slopes and intercepts of the linear regressions corresponding to these correlations are shown for comparison.

continental (including lower crustal) material into a "marble-cake"-like convective mantle (*e.g.*Varas-Reus et al., 2018). As such, they may explain the organization of asthenospheric heterogeneities documented by the linear EM trends of oceanic basalts in multi-isotopic and trace-element spaces (*e.g.*Chauvel et al., 1992; Agranier et al., 2005; Stracke, 2012).

Some recycling of continental material is required in most models of continental crust evolution (*e.g.*Belousova et al., 2010; Dhuime et al., 2018). Differentiation and gravitational removal (*i.e.* delamination) of dense magmatic products (mostly pyroxenites) of arcs is increasingly identified as a major tectonic process (Jagoutz and Kelemen, 2015; Ducea et al., 2020). However, this process, which potentially represents more than half of the magmatic arc flux in volume and one third of the subducted slabs globally (Jagoutz and Schmidt, 2013), has attracted little attention from the mantle community. The EM1 component and DUPAL-like anomalies have often been postulated as consequences of continental contamination (Stracke, 2012, and references therein) but the mechanisms for introducing continental material into the basalt sources are left unclear (*e.g.*Shirey et al., 1987; Doucelance et al., 2003). Lithospheric "remobilization" during plume-lithosphere interaction (Hawkesworth et al., 1986; Mahoney et al., 1989; Mahoney et al., 1992; Fontignie and Schilling, 1996; Widom et al., 1999) or continental breakup (Hoernle et al., 1991; Douglass et al., 1999; Douglass and Schilling, 2000; Andres et al., 2002; Escrig et al., 2004; Escrig et al., 2005a; Escrig et al., 2005b) have been widely proposed. However, delamination in this context only is viable if the SCLM is previously refertilized and thus negatively buoyant (*e.g.*Gibson et al., 2005; Geldmacher et al., 2008). Delamination in orogenic contexts has also been envisaged (McKenzie and O'nions, 1983; Lustrino, 2005), but only Tatsumi (2000) has modelled the impact of arc-root delamination. He focussed on Sr-Nd-Pb isotopes and thus only considered the origin of EM1, but extremely radiogenic Hf could be a distinctive, yet unexplored, isotopic signature of delaminated arc-derived material in the mantle.

Delamination of pyroxenite cumulates has been invoked to account for the similarity between garnet pyroxenite xenoliths and granitic batholiths from Sierra Nevada in California (Lee and Anderson, 2015). A recycled origin *via* delamination was proposed for Beni Bousera type-IV pyroxenites (*i.e.* garnet metagabbros) whose compositions are comparable to the lower-crustal cumulates from the Kohistan arc (Gysi et al., 2011). Perhaps the only direct example of delaminated pyroxenites that have escaped recycling is preserved in the Cabo Ortegal Complex in NW Spain, where the Herbeira massif is interpreted as an arc root delaminated due to the presence of abundant pyroxenites formed by magmatic segregation and melt-peridotite interaction in a harzburgitic mantle (Tilhac et al., 2016). Episodes of prograde metamorphism, high-temperature and high-shear strain deformation document the sinking and subsequent subduction and exhumation of the delaminated root (Tilhac et al., 2016; Henry et al., 2017; Tilhac, 2017; Tilhac et al., 2017). Osmium model ages up to 3 Ga and decoupled radiogenic Hf (Fig. 11a) imply that the pyroxenites inherited an ancient continental signature during the reworking of the northern margin of Gondwana by Cadomian arc magmatism (Tilhac et al., 2020).

As envisaged by Jagoutz and Schmidt (2013), arc-root delamination may introduce material with extremely radiogenic Hf, in contrast to the delamination of refertilized lithosphere with array-like Hf-Nd compositions. It provides an alternative petrological and tectonic scenario for the ancient, depleted component identified in the convective mantle from the variability in Hf isotopes between MOR segments (*i.e.* ReLish). Salters et al. (2011) initially ruled out the contribution of continental material to the ReLish because SCLM samples either have decoupled Hf-Nd isotopes and unradiogenic Nd or have low Hf/Nd when they exhibit coupled Hf-Nd depletion (Fig. 8b). Mixing with such compositions would primarily lead to a decrease in ε_{Nd} without significantly impacting ε_{Hf}, which is incompatible with the parallel arrays of MOR segments (Fig. 4b), although there is a rough inverse correlation between the average $\Delta\varepsilon_{Hf}$ of each segment and their Nd compositions (Fig. 11c). In contrast, Fig. 12 shows that mixing between a DM-like component and low-Hf material with decoupled Hf-Nd mostly affects Hf isotopes without significantly impacting Nd. The presence of such recycled continental material thus explains the vertical scatter in ε_{Nd}-ε_{Hf} space by combining a "continental" signature (*i.e.* highly radiogenic Hf) with Nd compositions comparable to oceanic basalts (Fig. 11b). This scenario is particularly plausible in the case of delamination of arc-related pyroxenites (Fig. 13a), which can preserve radiogenic Hf from the SCLM due to the low Hf/Nd of arc magmas (Fig. 6), as documented in the Cabo Ortegal Complex (Tilhac et al., 2020). Owing to the fertility of these lithologies (*e.g.*Lambart et al., 2016), pyroxenites could also become a preferential source of isotopically depleted melts carrying ancient, radiogenic Hf signatures. Sanfilippo et al. (2019) calculated that 15% of such melts can account for most of the Hf variability between MOR segments, which could thus directly or indirectly reflect variable contributions of pyroxenites to melting, a scenario somewhat similar to that envisaged by Ito and Mahoney (2005).

5.2.2. *Rifting and plume-lithosphere interaction processes*

We conclude this review by mentioning some Hf-Nd isotope case studies, mostly from the Alpine-Apennine ophiolites and Afro-Arabian mantle xenoliths, relevant to the introduction of continental material

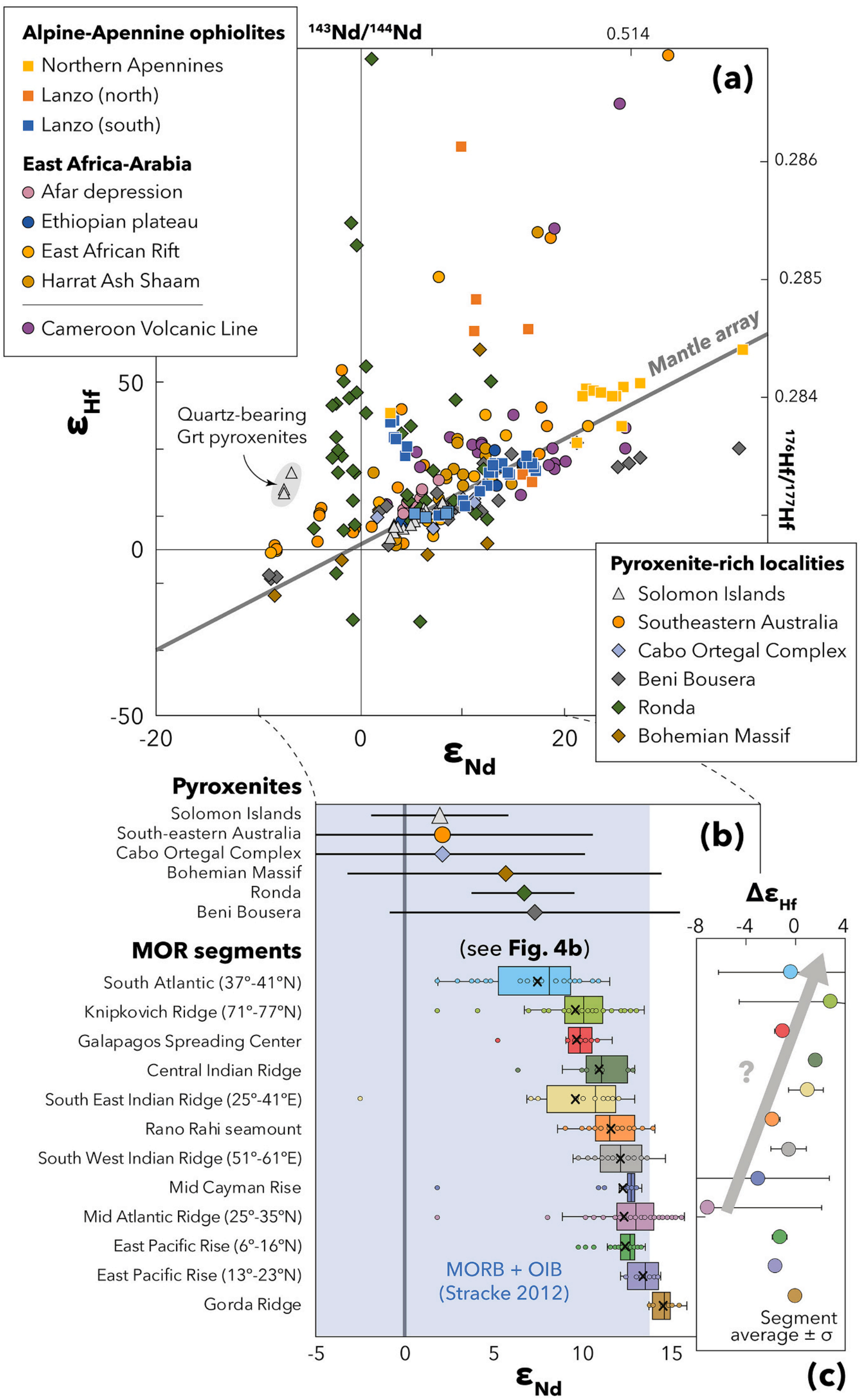

Fig. 11. (a) Plot of present-day ε_{Hf} *vs* ε_{Nd} for selected localities from the Alpine-Apennine ophiolites and basalt-borne xenoliths from the East African-Arabian region; the Xenoliths from the Cameroon Volcanic Line (CVL) as well as pyroxenite-rich localities from orogenic peridotite massifs and xenoliths from SE Australia and Malaita alnoïte in the Solomon Islands are also shown. Note the decoupled quartz-bearing garnet clinopyroxenites from the latter xenoliths contrasting with the rest of the samples plotting on the mantle array. Source references are listed in Tables 1a and 1b. (b) Box-and-whisker plot for the different MOR segments shown in Fig. 4b sorted by average Nd compositions, compared to average pyroxenite (± σ) compositions for the localities discussed in *Section 5.3.* The latter pyroxenites mostly overlap with MORB compositions and particularly with segments (*e.g.* South Atlantic, Knipkovitch) for which the highest proportions of ReLish are inferred (Sanfilippo et al., 2019); MORB and OIB compiled by Stracke (2012) are shown for comparison. (c) Average $\Delta\varepsilon_{Hf}$ (± σ) for each MOR segment shown in (b), outlining a potential correlation between Nd isotopes and $\Delta\varepsilon_{Hf}$ for most ridges.

into the sub-oceanic mantle during continental breakup; this extends previous discussions by Rampone and Hofmann (2012).

Ophiolites from the Alpine-Apennine belts in NW Italy are interpreted as remnants of the Alpine Tethys ocean and its ocean-continent transition zone, recording crust-mantle evolution during continental extension and processes at ultra-slow-spreading ridges (Rampone and Sanfilippo, 2021, and references therein). In the Northern Apennines, Sm-Nd and Lu-Hf isochrons in garnet pyroxenites have been used to constrain the mantle exhumation history based on P-T estimates and the relative closure temperatures of the two systems (Montanini et al., 2006). In the North Lanzo peridotites (Fig. 11a), positive decoupling of Hf and Nd isotopes documents both *syn*-rift percolation of HFSE-depleted alkali melts and the presence of an old SCLM affected by pre-rift melt percolation (Guarnieri et al., 2012). In contrast, the Hf-Nd decoupling observed in the replacive harzburgite bodies of South Lanzo has been interpreted as reflecting sub-ridge interaction between the host plagioclase lherzolites and isotopically depleted melts from an old (>1.2 Ga), potentially SCLM-derived refractory mantle (Sanfilippo et al., 2019; Rampone and Sanfilippo, 2021).

These examples suggest that continental breakup and rifting can introduce continental material into the oceanic lithosphere. However, the impact of this mechanism on the convective mantle is debated, as illustrated by the controversy (reminiscent of the “chicken-and-egg” dilemma discussed above) on the origin of the “continental” signatures

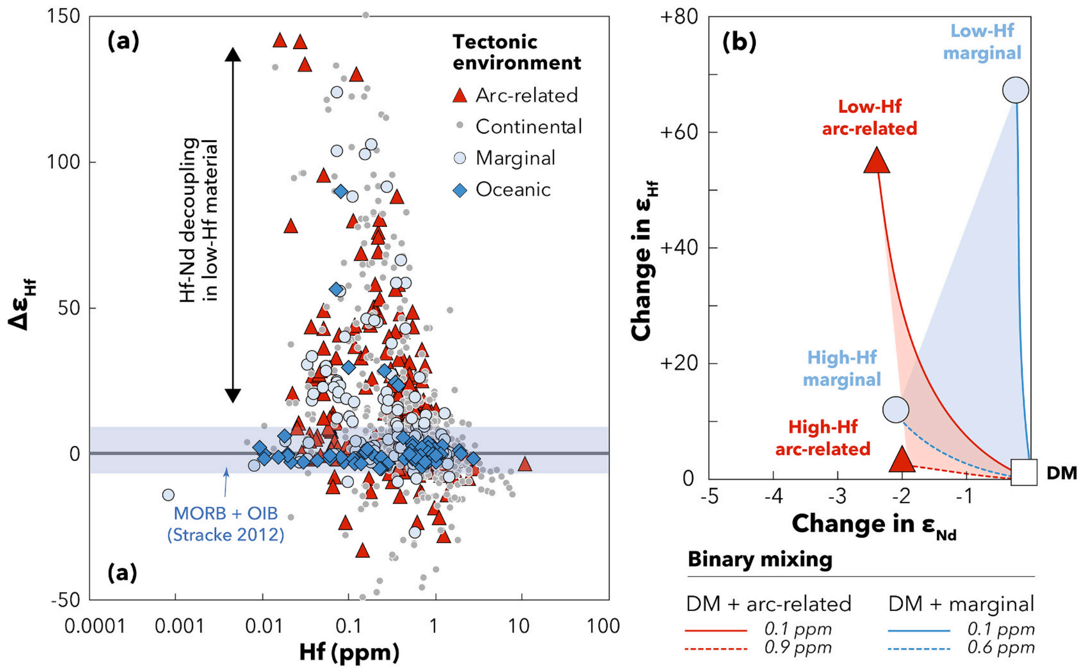

Fig. 12. (a) $\Delta\varepsilon_{Hf}$ *vs* Hf concentrations in the whole dataset discriminated based on tectonic affinity (as detailed in Tables 1a and 1b). Note the preferential decoupling towards radiogenic Hf at low-Hf concentrations. (b) Simple mixing models between representative compositions of arc-related and marginal terranes shown in (a) and a component with DM trace-element systematics. The plot shows the change in isotopic compositions compared to the DM-like component highlighting the fact that mixing with low-Hf material leads to a strong variability in ε_{Hf} (>50 ε_{Hf} units) at nearly constant ε_{Nd} (within 3 ε_{Nd} units). The starting compositions were obtained from the data plotted in (a) as follows: for both environments, average trace-element and isotope compositions were calculated for the data below (*low-Hf*) and above (*high-Hf*) the median Hf concentrations (0.39 ppm for arc-related and 0.19 ppm for marginal terranes).

identified in the ultraslow-spreading Gakkel ridge. These have been alternatively interpreted as due to (1) the presence of ultra-depleted domains in the convective mantle based on ancient Hf-Os depletion ages in AP (Liu et al., 2008; Stracke et al., 2011), (2) SCLM material delaminated beneath the Arctic during continental breakup identified from DUPAL-like anomalies in Gakkel ridge basalts (Goldstein et al., 2008) or (3) recent incorporation of stranded blocks of SCLM and crustal remnants (*i.e.* most likely never subjected to convection) during the opening of the northern Atlantic Ocean (Griffin et al., 2012). In favour of the latter interpretation, we note that the Gakkel ridge lies directly along the eastward trajectory of the Svalbard block following its separation from northern Greenland, and that Svalbard may have lost its Archean root (although this point is debated; Choi et al., 2010), as suggested by a clear dichotomy in sulfide age populations in the Spitsbergen xenoliths (Griffin et al., 2012). In fact, the Hf-isotope compositions of MORB from the Mohns to Knipovich ridges also increase as the distance to Svalbard archipelago decreases (Sanfilippo et al., 2021), most likely reflecting contamination with continental material (*e.g.* Blichert-Toft et al., 2005). The garnet signature observed in spinel-facies peridotite xenoliths with Neoproterozoic to Archean sulfide-Os model ages from the Cape Verde archipelago can be similarly explained in relation to the opening of the central Atlantic Ocean (Bonadiman et al., 2005; Coltorti et al., 2010). Continental fragments (including crustal rocks) are also found in the South Atlantic Ocean (Milner and le Roex, 1996; Kamenetsky et al., 2001; Santos et al., 2019).

Continental dispersal tends to be limited to the shallow sub-oceanic mantle when it affects buoyant, refractory material unlikely to be recycled in the convective mantle (Fig. 13b), even during plume-lithosphere interaction (*e.g.* Class and le Roex, 2006; Liu et al., 2022). For instance, the impingement of the Afar plume beneath the Ethiopian plateau has not apparently led to complete removal of the SCLM (Alemayehu et al., 2017). In contrast, the introduction of marginal SCLM into the convective mantle can be envisaged provided that the SCLM was previously refertilized (*e.g.* Gibson et al., 2005; Geldmacher et al., 2008). However, in such cases the originally depleted signatures are likely to be strongly overprinted by arc magmatism, as suggested by the similar range of positively decoupled Hf isotopes in terranes of arc-related and marginal affinities (Fig. 12a), and cannot account for the depleted components identified in oceanic basalts. Rheological contrasts constrain the development of rift structures to pre-existing sutures along craton margins, which tend to be preferentially refertilized and hence gravitationally unstable (*e.g.* Petit and Ebinger, 2000; Begg et al., 2009; Corti, 2013). Regional extension (back-arc rifting) can also be driven by flat-slab episodes followed by slab steepening (Sdrolias and Müller, 2006). For instance, in the Cenozoic East African Rift (Le Gall et al., 2008; Hammond et al., 2013), ancient depletion and metasomatic processes are documented in the Ethiopian segments of the rift (Bianchini et al., 2014; Alemayehu et al., 2017), corresponding to a major lithospheric discontinuity between the Tanzanian craton and the Pan-African belt (Begg et al., 2009). The pre-rifting history of the Afro-Arabian lithosphere also includes carbonatitic metasomatism associated with the Pan-African subduction identified in xenoliths from NW Jordan by decoupled Hf-Nd isotopes (Fig. 11a), correlations between Sr-Nd-Pb isotopes and HFSE depletion (Shaw et al., 2007). Similar signatures overprinted by recent plume-related metasomatism are found beneath the nearby Ethiopian plateau (Alemayehu et al., 2017); the latter localities are accordingly classified as T/P and T/P/A (Tables 1a and 1b). In contrast to the Jordanian and Ethiopian samples, xenoliths from the Assab volcanic field in the Afar depression are characterized by (re-)coupled Hf and Nd isotopes yielding isochrons nearly identical to the 30-Ma reference lines, and interpreted as related to the Afar plume (Teklay et al., 2010). Other examples of tectonic reactivation in rift systems include the Jemez Lineament in the western USA (Tilhac et al., 2021), a “lithospheric memory” of subduction identified in rift-related basalt-borne xenoliths of SE Australia (Lu et al., 2018; Lu et al., 2020) or old Hf-Os ages in xenoliths from the Cameroon Volcanic Line (Liu et al., 2017a; Liu et al., 2019), which extends along a Pan-African belt separating cratonic blocks.

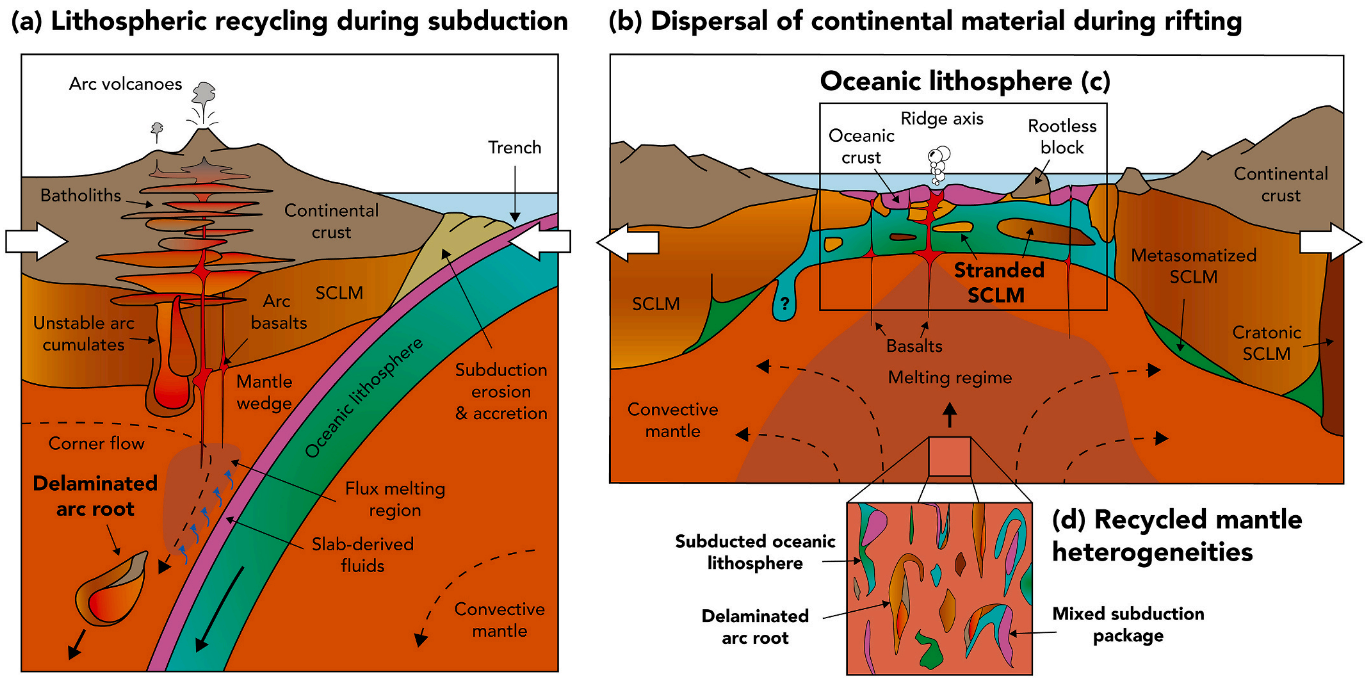

Fig. 13. Schematic representation of the main tectonic scenarios proposed for the recycling of continental material into the sub-oceanic and convective mantle. (a) Recycling of continental and oceanic lithosphere in a subduction zone where delamination of gravitationally unstable arc cumulates represent a potentially important means of introducing pyroxenites into the convective mantle. Delaminated products are likely to carry a continental signature inherited when arcs develop on continental margins where arc magmas may interact with old SCLM. The Herbeira massif of the Cabo Ortegal Complex may represent an exhumed analogue of such a delaminated arc root. (b) Continental dispersal following continental breakup along pre-existing lithospheric discontinuities. Shades of green/blue in the sub-oceanic and sub-continental lithospheric mantle illustrate variations in fertility/degree of refertilization; shades of brown in SCLM illustrate variations in degree of depletion reflecting its tectono-thermal history. Analogues of the Svalbard-Gakkel connection discussed in the text are illustrated by the rootless block (Svalbard archipelago) and the ridge sampling stranded SCLM (Gakkel ridge). The inheritance of SCLM-derived heterogeneities in the sub-oceanic mantle is also documented in the Alpine-Apennine ophiolites. The introduction of continental material by rifting is restricted to the lithosphere unless the SCLM had been made negatively buoyant by previous refertilization by previous subduction-related episodes. In (a), the subducting oceanic lithosphere must also be internally heterogeneous (not shown) as a consequence of the processes taking place during rifting (c). Subduction-derived heterogeneities are recycled in the convective mantle (d) where convection stirring may result in the formation of mixtures of recycled continental and oceanic products as reflected by the diversity of pyroxenites in the Beni Bousera and Ronda massifs. The source of isotopically ancient/depleted signature identified in oceanic basalts and abyssal peridotites may thus be lithospheric (c) and/or asthenospheric (d). Complexities arising from plume-lithosphere interaction are omitted for clarity. (For interpretation of the references to colour in this figure legend, the reader is referred to the web version of this article.)

6. Concluding remarks and future perspectives

This review of all Hf and Nd-isotope data published to date on mantle peridotites and pyroxenites provides a comprehensive view of the petrological and tectonic processes controlling global Hf-Nd isotope systematics, and in particular the decoupling between these two isotope systems. Positive decoupling (*i.e.* above the Hf-Nd mantle array) is ubiquitous in both peridotites and pyroxenites and can generally be regarded as reflecting (transient) melt-peridotite interaction involving ancient, depleted material whose Hf-isotope ratios (and protolith ages) may be underestimated. However, coupled or negatively decoupled Hf-Nd isotopes, particularly in recycled pyroxenites such as those of the Beni Bousera and Ronda massifs, certainly cannot rule out the involvement of ancient protoliths.

Our discussion builds on previous contributions by Rampone and Hofmann (2012) and Stracke (2012) on the origin of the depleted material identified from oceanic volcanics and abyssal peridotites. Global Hf-Nd isotope systematics indicate that delamination of the lithospheric root of magmatic arcs developed along continental margins, and to a lesser extent (*i.e.* limited to the oceanic lithosphere) SCLM dispersal following continental breakup/collision cycles are the dominant means of introducing ancient continental material into the sub-oceanic mantle. Several lines of evidence support these conclusions.

- Continental lithosphere, particularly when reworked by arc magmatism, can exhibit extremely radiogenic Hf isotopes, comparable to the depleted component inferred from MORB (Salters et al., 2011) and to material directly sampled in AP (Stracke et al., 2011) or by OIB, such as in Hawaii. Pristine Archean mantle, in contrast, often has sub-chondritic Nd isotopes.
- There is increasing evidence for the presence of arc−/continent-derived material in the sub-oceanic mantle. For instance, highly depleted peridotites interpreted as recycled (sub-arc) flux-melting residues were recovered from the mid-Atlantic ridge (Urann et al., 2020) – see also le Roux et al. (2002). Paleoproterozoic to Neoarchean T_{RD} were also recently reported in AP from the SWIR (Liu et al., 2022). In Hawaii, Cretaceous U-Pb ages and Proterozoic Hf model ages in zircons from xenoliths remarkably suggest a subcontinental derivation (Greenough et al., 2021) and recycled pyroxenites are invoked as a carbonated source of rejuvenated-stage volcanics (Borisova and Tilhac, 2021).
- Arc-root delamination provides a significant flux of mafic material (*i. e.* pyroxenites) into the convective mantle, potentially representing more than twice the mass of arc crust produced (Jagoutz and Schmidt, 2013) – see also Lee and Anderson (2015). It is reasonable to envisage that this mass flux has had significant consequences for the mantle's long-term isotopic evolution.

These conclusions support the concept that (1) subduction is the main driving force controlling the major mass transfers between the oceanic and continental lithosphere and convective mantle (Stracke, 2012), and (2) the long-term evolution of the continental crust and the compositional differentiation of the mantle are directly related to plate-tectonic processes at convergent plate margins, at least since the Archean. The dataset provided here is a robust basis to constrain the long-term temporal evolution of the Earth's major geochemical reservoirs. Other major conclusions of this review are to (3) reconcile the apparent contradiction between the homogeneity of oceanic basalts and the diversity and complexity of their source rocks, and (4) highlight that fertile lithologies such as pyroxenites may well carry extremely depleted isotopic signatures. Building on previous works (*e.g.*Lambart et al., 2012; Lambart et al., 2016; Brunelli et al., 2018; Elkins et al., 2019; Oliveira et al., 2020), a better characterization of mixed-source melting relationships is needed to fully envisage the consequences of lithospheric recycling. Following Shu et al. (2013, 2014), further efforts should also be dedicated to better deconvolve the geochronological *versus* mixing relationships that underpin a surprising amount of the "chicken-and-egg" debate on ancient mantle signatures.

Declaration of Competing Interest

The authors declare that they have no known competing financial interests or personal relationships that could have appeared to influence the work reported in this paper.

Acknowledgements

We are grateful to T. Morishita and C.J. Garrido for their support during the laborious elaboration of the database and writing of the manuscript. We thank A. Sanfilippo for providing data for the individual MOR segments. Constructive comments and suggestions by M. Bizimis, an anonymous reviewer and the editor C. Chauvel greatly improved the manuscript. Romain Tilhac acknowledges grant FJC2018-036729 funded by MCIN/AEI/10.13039/501100011033 and "ESF, Investing in your future" and grant AEI-PID2021-122792NA-I00 funded by MCIN/AEI/10.13039/501100011033 and "ERDF, A way of making Europe". This is contribution 1742 from the ARC Centre of Excellence for Core to Crust Fluid Systems (http://www.ccfs.mq.edu.au) and 1511 from the GEMOC Key Centre (http://www.gemoc.mq.edu.au).

Appendix A. Supplementary data

Supplementary data to this article can be found online at https://doi.org/10.1016/j.chemgeo.2022.121039.

References

Ackerman, L., Bizimis, M., Haluzová, E., Sláma, J., Svojtka, M., Hirajima, T., Erban, V., 2016. Re–Os and Lu–Hf isotopic constraints on the formation and age of mantle pyroxenites from the Bohemian Massif. Lithos 256–257, 197–210.

Ackerman, L., Kotková, J., Čopjaková, R., Sláma, J., Trubač, J., Dillingerová, V., 2020. Petrogenesis and Lu–Hf Dating of (Ultra)Mafic Rocks from the Kutná Hora Crystalline complex: implications for the Devonian Evolution of the Bohemian Massif. J. Petrol. 61.

Agranier, A., Blichert-Toft, J., Graham, D., Debaille, V., Schiano, P., Albarède, F., 2005. The spectra of isotopic heterogeneities along the mid-Atlantic Ridge. Earth Planet. Sci. Lett. 238, 96–109.

Alard, O., Luguet, A., Pearson, N.J., Griffin, W.L., Lorand, J.-P., Gannoun, A., Burton, K. W., O'Reilly, S.Y., 2005. In situ Os isotopes in abyssal peridotites bridge the isotopic gap between MORBs and their source mantle. Nature 436, 1005–1008.

Albarède, F., Simonetti, A., Vervoort, J.D., Blichert-Toft, J., Abouchami, W., 1998. A Hf-Nd isotopic correlation in ferromanganese nodules. Geophys. Res. Lett. 25, 3895–3898.

Albarède, F., Blichert-Toft, J., Vervoort, J.D., Gleason, J.D., Rosing, M., 2000. Hf–Nd isotope evidence for a transient dynamic regime in the early terrestrial mantle. Nature 404, 488.

Alemayehu, M., Zhang, H.-F., Aulbach, S., 2017. Persistence of fertile and hydrous lithospheric mantle beneath the northwestern Ethiopian plateau: evidence from modal, trace element and Sr–Nd–Hf isotopic compositions of amphibole-bearing mantle xenoliths. Lithos 284–285, 401–415.

Allègre, C.J., Hamelin, B., Dupré, B., 1984. Statistical analysis of isotopic ratios in MORB: the mantle blob cluster model and the convective regime of the mantle. Earth Planet. Sci. Lett. 71, 71–84.

Andres, M., Blichert-Toft, J., Schilling, J.-G., 2002. Hafnium isotopes in basalts from the southern Mid-Atlantic Ridge from 40°S to 55°S: discovery and Shona plume-ridge interactions and the role of recycled sediments. Geochem. Geophys. Geosyst. 3, 1–25.

Armienti, P., Gasperini, D., 2007. Do we really need mantle components to define mantle composition? J. Petrol. 48, 693–709.

Arndt, N.T., Goldstein, S.L., 1989. An open boundary between lower continental crust and mantle: its role in crust formation and crustal recycling. Tectonophysics 161, 201–212.

Asimow, P.D., Langmuir, C.H., 2003. The importance of water to oceanic mantle melting regimes. Nature 421, 815.

Aulbach, S., Griffin, W., O'Reilly, S., McCandless, T.E., 2004. Genesis and evolution of the lithospheric mantle beneath the Buffalo Head Terrane, Alberta (Canada). Lithos 77, 413–451.

Bayon, G., Burton, K.W., Soulet, G., Vigier, N., Dennielou, B., Etoubleau, J., Ponzevera, E., German, C.R., Nesbitt, R.W., 2009. Hf and Nd isotopes in marine sediments: constraints on global silicate weathering. Earth Planet. Sci. Lett. 277, 318–326.

Bayon, G., Skonieczny, C., Delvigne, C., Toucanne, S., Bermell, S., Ponzevera, E., André, L., 2016. Environmental Hf–Nd isotopic decoupling in World river clays. Earth Planet. Sci. Lett. 438, 25–36.

Beard, B.L., Medaris, L.G., Johnson, C.M., Brueckner, H.K., Mísař, Z., 1992. Petrogenesis of Variscan high-temperature Group a eclogites from the Moldanubian Zone of the Bohemian Massif, Czechoslovakia. Contrib. Mineral. Petrol. 111, 468–483.

Beccaluva, L., Bianchini, G., Ellam, R.M., Natali, C., Santato, A., Siena, F., Stuart, F.M., 2011. Peridotite xenoliths from Ethiopia: Inferences about mantle processes from plume to rift settings. Volcanism Evol. Afr. Lithos. 77–104.

Bedini, R.M., Blichert-Toft, J., Boyet, M., Albarède, F., 2004. Isotopic constraints on the cooling of the continental lithosphere. Earth Planet. Sci. Lett. 223, 99–111.

Begemann, F., Ludwig, K.R., Lugmair, G.W., Min, K., Nyquist, L.E., Patchett, P.J., Renne, P.R., Shih, C.Y., Villa, I.M., Walker, R.J., 2001. Call for an improved set of decay constants for geochronological use. Geochim. Cosmochim. Acta 65, 111–121.

Begg, G.C., Griffin, W.L., Natapov, L.M., O'Reilly, S.Y., Grand, S.P., O'Neill, C.J., Hronsky, J.M.A., Djomani, Y.P., Swain, C.J., Deen, T., Bowden, P., 2009. The lithospheric architecture of Africa: Seismic tomography, mantle petrology, and tectonic evolution. Geosphere 5, 23–50.

Béguelin, P., Bizimis, M., Beier, C., Turner, S., 2017. Rift–plume interaction reveals multiple generations of recycled oceanic crust in Azores lavas. Geochim. Cosmochim. Acta 218, 132–152.

Belousova, E.A., Kostitsyn, Y.A., Griffin, W.L., Begg, G.C., O'Reilly, S.Y., Pearson, N.J., 2010. The growth of the continental crust: constraints from zircon Hf-isotope data. Lithos 119, 457–466.

Ben Othman, D., White, W.M., Patchett, J., 1989. The geochemistry of marine sediments, island arc magma genesis, and crust-mantle recycling. Earth Planet. Sci. Lett. 94, 1–21.

Bianchini, G., Beccaluva, L., Bonadiman, C., Nowell, G., Pearson, G., Siena, F., Wilson, M., 2007. Evidence of diverse depletion and metasomatic events in harzburgite–lherzolite mantle xenoliths from the Iberian plate (Olot, NE Spain): implications for lithosphere accretionary processes. Lithos 94, 25–45.

Bianchini, G., Bryce, J.G., Blichert-Toft, J., Beccaluva, L., Natali, C., 2014. Mantle dynamics and secular variations beneath the East African Rift: insights from peridotite xenoliths (Mega, Ethiopia). Chem. Geol. 386, 49–58.

Bizimis, M., Sen, G., Salters, V.J.M., 2003. Hf–Nd isotope decoupling in the oceanic lithosphere: constraints from spinel peridotites from Oahu, Hawaii. Earth Planet. Sci. Lett. 217, 43–58.

Bizimis, M., Sen, G., Salters, V.J., Keshav, S., 2005. Hf-Nd-Sr isotope systematics of garnet pyroxenites from Salt Lake Crater, Oahu, Hawaii: evidence for a depleted component in Hawaiian volcanism. Geochim. Cosmochim. Acta 69, 2629–2646.

Bizimis, M., Griselin, M., Lassiter, J.C., Salters, V.J.M., Sen, G., 2007. Ancient recycled mantle lithosphere in the Hawaiian plume: Osmium–Hafnium isotopic evidence from peridotite mantle xenoliths. Earth Planet. Sci. Lett. 257, 259–273.

Bizzarro, M., Simonetti, A., Stevenson, R.K., David, J., 2002. Hf isotope evidence for a hidden mantle reservoir. Geology 30, 771–774.

Blichert-Toft, J., Albarède, F., 1997. The Lu-Hf isotope geochemistry of chondrites and the evolution of the mantle-crust system. Earth Planet. Sci. Lett. 148, 243–258.

Blichert-Toft, J., Albarède, F., Kornprobst, J., 1999. Lu-Hf isotope systematics of garnet pyroxenites from Beni Bousera, Morocco: implications for basalt origin. Science 283, 1303–1306.

Blichert-Toft, J., Agranier, A., Andres, M., Kingsley, R., Schilling, J.-G., Albarède, F., 2005. Geochemical segmentation of the Mid-Atlantic Ridge north of Iceland and ridge–hot spot interaction in the North Atlantic. Geochem. Geophys. Geosyst. 6 n/a-n/a.

Bloch, E., Ganguly, J., 2014. 176Lu–176Hf and 147Sm–143Nd ages of the Martian shergottites: Evaluation of the shock-resetting hypothesis through diffusion kinetic experiments and modeling, and petrological observations. Earth Planet. Sci. Lett. 395, 173–183.

Blundy, J.D., Robinson, J.A.C., Wood, B.J., 1998. Heavy REE are compatible in clinopyroxene on the spinel lherzolite solidus. Earth Planet. Sci. Lett. 160, 493–504.

Bonadiman, C., Beccaluva, L., Coltorti, M., Siena, F., 2005. Kimberlite-like Metasomatism and 'Garnet Signature' in Spinel-peridotite Xenoliths from Sal, Cape Verde Archipelago: relics of a subcontinental mantle domain within the atlantic oceanic lithosphere? J. Petrol. 46, 2465–2493.

Borghini, G., Rampone, E., Class, C., Goldstein, S., Cai, Y., Cipriani, A., Hofmann, A.W., Bolge, L., 2021. Enriched Hf Nd isotopic signature of veined pyroxenite-infiltrated peridotite as a possible source for E-MORB. Chem. Geol. 586.

Borisova, A.Y., Tilhac, R., 2021. Derivation of Hawaiian rejuvenated magmas from deep carbonated mantle sources: a review of experimental and natural constraints. Earth Sci. Rev. 222.

Bouvier, A., Vervoort, J.D., Patchett, P.J., 2008. The Lu–Hf and Sm–Nd isotopic composition of CHUR: constraints from unequilibrated chondrites and implications for the bulk composition of terrestrial planets. Earth Planet. Sci. Lett. 273, 48–57.

Bragagni, A., Luguet, A., Fonseca, R.O.C., Pearson, D.G., Lorand, J.P., Nowell, G.M., Kjarsgaard, B.A., 2017. The geological record of base metal sulfides in the cratonic mantle: a microscale 187 Os/ 188 Os study of peridotite xenoliths from Somerset Island, Rae Craton (Canada). Geochim. Cosmochim. Acta 216, 264–285.

Brandon, A.D., Snow, J.E., Walker, R.J., Morgan, J.W., Mock, T.D., 2000. 190Pt–186Os and 187Re–187Os systematics of abyssal peridotites. Earth Planet. Sci. Lett. 177, 319–335.

Brunelli, D., Cipriani, A., Bonatti, E., 2018. Thermal effects of pyroxenites on mantle melting below mid-ocean ridges. Nat. Geosci. 11, 520–525.

Byerly, B.L., Lassiter, J.C., 2012. Evidence from mantle xenoliths for lithosphere removal beneath the Central Rio Grande Rift. Earth Planet. Sci. Lett. 355-356, 82–93.

Byerly, B.L., Lassiter, J.C., 2014. Isotopically ultradepleted domains in the convecting upper mantle: Implications for MORB petrogenesis. Geology 42, 203–206.

Byerly, B.L., Lassiter, J.C., 2015. Trace element partitioning and Lu–Hf isotope systematics in spinel peridotites from the Rio Grande Rift and Colorado Plateau: Towards improved age assessment of clinopyroxene Lu/Hf–176Hf/177Hf in SCLM peridotite. Chem. Geol. 413, 146–158.

Carlson, R.W., Ionov, D.A., 2019. Compositional characteristics of the MORB mantle and bulk silicate earth based on spinel peridotites from the Tariat Region, Mongolia. Geochim. Cosmochim. Acta 257, 206–223.

Carlson, R.W., Irving, A.J., Schulze, D.J., Hearn, B.C., 2004. Timing of Precambrian melt depletion and Phanerozoic refertilization events in the lithospheric mantle of the Wyoming Craton and adjacent Central Plains Orogen. Lithos 77, 453–472.

Chauvel, C., Blichert-Toft, J., 2001. A hafnium isotope and trace element perspective on melting of the depleted mantle. Earth Planet. Sci. Lett. 190, 137–151.

Chauvel, C., Hofmann, A.W., Vidal, P., 1992. HIMU-EM: the French Polynesian connection. Earth Planet. Sci. Lett. 110, 99–119.

Chauvel, C., Lewin, E., Carpentier, M., Arndt, N.T., Marini, J.-C., 2008. Role of recycled oceanic basalt and sediment in generating the Hf-Nd mantle array. Nat. Geosci. 1, 64–67.

Chauvel, C., Marini, J.-C., Plank, T., Ludden, J.N., 2009. Hf-Nd input flux in the Izu-Mariana subduction zone and recycling of subducted material in the mantle. Geochem. Geophys. Geosyst. 10, n/a–n/a.

Cheng, H., King, R.L., Nakamura, E., Vervoort, J.D., Zhou, Z., 2008. Coupled Lu–Hf and Sm–Nd geochronology constrains garnet growth in ultra-high-pressure eclogites from the Dabie orogen. J. Metamorph. Geol. 26, 741–758.

Choi, S.H., Mukasa, S.B., 2012. Lu–Hf and Sm–Nd isotope systematics of Korean spinel peridotites: a case for metasomatically induced Nd–Hf decoupling. Lithos 154, 263–276.

Choi, S.H., Kwon, S.-T., Mukasa, S.B., Sagong, H., 2005. Sr–Nd–Pb isotope and trace element systematics of mantle xenoliths from late Cenozoic alkaline lavas, South Korea. Chem. Geol. 221, 40–64.

Choi, S.H., Mukasa, S.B., Andronikov, A.V., Marcano, M.C., 2007. Extreme Sr–Nd–Pb–Hf isotopic compositions exhibited by the Tinaquillo peridotite massif, Northern Venezuela: implications for geodynamic setting. Contrib. Mineral. Petrol. 153, 443–463.

Choi, S.H., Mukasa, S.B., Zhou, X.-H., Xian, X.H., Andronikov, A.V., 2008. Mantle dynamics beneath East Asia constrained by Sr, Nd, Pb and Hf isotopic systematics of ultramafic xenoliths and their host basalts from Hannuoba, North China. Chem. Geol. 248, 40–61.

Choi, S.H., Suzuki, K., Mukasa, S.B., Lee, J.-I., Jung, H., 2010. Lu–Hf and Re–Os systematics of peridotite xenoliths from Spitsbergen, western Svalbard: implications for mantle–crust coupling. Earth Planet. Sci. Lett. 297, 121–132.

Chu, Z.-Y., Wu, F.-Y., Walker, R.J., Rudnick, R.L., Pitcher, L., Puchtel, I.S., Yang, Y.-H., Wilde, S.A., 2009. Temporal evolution of the lithospheric mantle beneath the Eastern North China Craton. J. Petrol. 50, 1857–1898.

Cipriani, A., Brueckner, H.K., Bonatti, E., Brunelli, D., 2004. Oceanic crust generated by elusive parents: Sr and Nd isotopes in basalt-peridotite pairs from the Mid-Atlantic Ridge. Geology 32, 657–660.

Class, C., le Roex, A.P., 2006. Continental material in the shallow oceanic mantle—how does it get there? Geology 34.

Coltorti, M., Bonadiman, C., O'Reilly, S.Y., Griffin, W.L., Pearson, N.J., 2010. Buoyant ancient continental mantle embedded in oceanic lithosphere (Sal Island, Cape Verde Archipelago). Lithos 120, 223–233.

Corentin, P., Pucéat, E., Pellenard, P., Freslon, N., Guiraud, M., Blondet, J., Adatte, T., Bayon, G., 2022. Hafnium-neodymium isotope evidence for enhanced weathering and uplift-climate interactions during the late cretaceous. Chem. Geol. 591, 120724.

Corti, G., 2013. Experimental modeling of rifting at cratonc margins. Geosphere 9.

Dhuime, B., Hawkesworth, C.J., Delavault, H., Cawood, P.A., 2018. Rates of generation and destruction of the continental crust: implications for continental growth. Philos Trans a Math Phys. Eng. Sci. 376.

Doucelance, R., Escrig, S., Moreira, M., Gariépy, C., Kurz, M.D., 2003. Pb-Sr-he isotope and trace element geochemistry of the Cape Verde Archipelago. Geochim. Cosmochim. Acta 67, 3717–3733.

Doucet, L.S., Ionov, D.A., Golovin, A.V., 2015. Paleoproterozoic formation age for the Siberian cratonic mantle: Hf and Nd isotope data on refractory peridotite xenoliths from the Udachnaya kimberlite. Chem. Geol. 391, 42–55.

Douglass, J., Schilling, J.G., 2000. Systematics of three-component, pseudo-binary mixing lines in 2D isotope ratio space representations and implications for mantle plume–ridge interaction. Chem. Geol. 163, 1–23.

Douglass, J., Schilling, J.G., Fontignie, D., 1999. Plume-ridge interactions of the discovery and Shona mantle plumes with the southern Mid-Atlantic Ridge (40°-55° S). J. Geophys. Res. Solid Earth 104, 2941–2962.

Downes, H., Dupuy, C., 1987. Textural, isotopic and REE variations in spinel peridotite xenoliths, Massif Central, France. Earth Planet. Sci. Lett. 82, 121–135.

Downes, H., Reichow, M.K., Mason, P.R.D., Beard, A.D., Thirlwall, M.F., 2003. Mantle domains in the lithosphere beneath the French Massif Central: trace element and isotopic evidence from mantle clinopyroxenes. Chem. Geol. 200, 71–87.

Ducea, M.N., Chapman, A.D., Bowman, E., Balica, C., 2020. Arclogites and their role in continental evolution; part 2: Relationship to batholiths and volcanoes, density and foundering, remelting and long-term storage in the mantle. Earth Sci. Rev. 214, 103476.

Dupré, B., Allègre, C.J., 1983. Pb–Sr isotope variation in Indian Ocean basalts and mixing phenomena. Nature 303, 142.

Elkins, L.J., Bourdon, B., Lambart, S., 2019. Testing pyroxenite versus peridotite sources for marine basalts using U-series isotopes. Lithos 332-333, 226–244.

Elliott, T., Zindler, A., Bourdon, B., 1999. Exploring the kappa conundrum: the role of recycling in the lead isotope evolution of the mantle. Earth Planet. Sci. Lett. 169, 129–145.

Escrig, S., Capmas, F., Dupré, B., Allègre, C., 2004. Osmium isotopic constraints on the nature of the DUPAL anomaly from Indian mid-ocean-ridge basalts. Nature 431, 59–63.

Escrig, S., Doucelance, R., Moreira, M., Allègre, C.J., 2005a. Os isotope systematics in Fogo Island: evidence for lower continental crust fragments under the Cape Verde Southern Islands. Chem. Geol. 219, 93–113.

Escrig, S., Schiano, P., Schilling, J.-G., Allègre, C., 2005b. Rhenium–osmium isotope systematics in MORB from the Southern Mid-Atlantic Ridge (40°–50° S). Earth Planet. Sci. Lett. 235, 528–548.

Fitzpayne, A., Giuliani, A., Hergt, J., Woodhead, J.D., Maas, R., 2020. Isotopic analyses of clinopyroxenes demonstrate the effects of kimberlite melt metasomatism upon the lithospheric mantle. Lithos 370–371.

Fitzpayne, A., Giuliani, A., Maas, R., Hergt, J., Janney, P., Phillips, D., 2019. Progressive metasomatism of the mantle by kimberlite melts: Sr–Nd–Hf–Pb isotope compositions of MARID and PIC minerals. Earth Planet. Sci. Lett. 509, 15–26.

Foley, S.F., Barth, M.G., Jenner, G.A., 2000. Rutile/melt partition coefficients for trace elements and an assessment of the influence of rutile on the trace element characteristics of subduction zone magmas. Geochim. Cosmochim. Acta 64, 933–938.

Fontignie, D., Schilling, J.-G., 1996. Mantle heterogeneities beneath the South Atlantic: a NdSrPb isotope study along the Mid-Atlantic Ridge (3°S–46°S). Earth Planet. Sci. Lett. 142, 209–221.

Frisby, C., Bizimis, M., Mallick, S., 2016a. Hf–Nd isotope decoupling in bulk abyssal peridotites due to serpentinization. Chem. Geol. 440, 60–72.

Frisby, C., Bizimis, M., Mallick, S., 2016b. Seawater-derived rare earth element addition to abyssal peridotites during serpentinization. Lithos 248–251, 432–454.

Fujimaki, H., 1986. Partition coefficients of Hf, Zr, and REE between zircon, apatite, and liquid. Contrib. Mineral. Petrol. 94, 42–45.

Gao, S., Luo, T.-C., Zhang, B.-R., Zhang, H.-F., Han, Y.-W., Zhao, Z.-D., Hu, Y.-K., 1998. Chemical composition of the continental crust as revealed by studies in East China. Geochim. Cosmochim. Acta 62, 1959–1975.

Gao, S., Rudnick, R.L., Yuan, H.-L., Liu, X.-M., Liu, Y.-S., Xu, W.-L., Ling, W.-L., Ayers, J., Wang, X.-C., Wang, Q.-H., 2004. Recycling lower continental crust in the North China craton. Nature 432, 892–897.

Garçon, M., Chauvel, C., France-Lanord, C., Huyghe, P., Lavé, J., 2013. Continental sedimentary processes decouple Nd and Hf isotopes. Geochim. Cosmochim. Acta 121, 177–195.

Gardiner, N.J., Johnson, T.E., Kirkland, C.L., Szilas, K., 2019. Modelling the Hafnium–Neodymium evolution of early Earth: a study from West Greenland. J. Petrol. 60, 177–197.

Geldmacher, J., Hoernle, K., Klügel, A., van den Bogaard, P., Bindeman, I., 2008. Geochemistry of a new enriched mantle type locality in the northern hemisphere: Implications for the origin of the EM-I source. Earth Planet. Sci. Lett. 265, 167–182.

Gibson, S.A., Thompson, R.N., Day, J.A., Humphris, S.E., Dickin, A.P., 2005. Melt-generation processes associated with the Tristan mantle plume: Constraints on the origin of EM-1. Earth Planet. Sci. Lett. 237, 744–767.

Giuliani, A., Phillips, D., Woodhead, J.D., Kamenetsky, V.S., Fiorentini, M.L., Maas, R., Soltys, A., Armstrong, R.A., 2015. Did diamond-bearing orangeites originate from MARID-veined peridotites in the lithospheric mantle? Nat. Commun. 6, 6837.

Gjata, K., Kornprobst, J., Kodra, A., Briot, D., Pineau, F., 1992. Subduction chaude a l'aplomb d'une dorsale? Exemple des enclaves de pyroxenite a grenat de la breche serpentineuse de Derveni (Albanie). Bull. Soc. Geol. Fr. 163, 469–476.

Goldstein, S.L., Soffer, G., Langmuir, C.H., Lehnert, K.A., Graham, D.W., Michael, P.J., 2008. Origin of a 'Southern Hemisphere' geochemical signature in the Arctic upper mantle. Nature 453, 89–93.

Gonzaga, R.G., Menzies, M.A., Thirlwall, M.F., Jacob, D.E., Leroex, A., 2010. Eclogites and garnet pyroxenites: problems resolving provenance using Lu–Hf, Sm–Nd and Rb–Sr isotope systems. J. Petrol. 51, 513–535.

Gréau, Y., Alard, O., Griffin, W.L., Huang, J.-X., O'Reilly, S.Y., 2013. Sulfides and chalcophile elements in Roberts Victor eclogites: Unravelling a sulfide-rich metasomatic event. Chem. Geol. 354, 73–92.

Greenough, J.D., Kamo, S.L., Davis, D.W., Larson, K., Zhang, Z., Layton-Matthews, D., De Vera, J., Bergquist, B.A., 2021. Old subcontinental mantle zircon below Oahu. Commun. Earth Environ. 2.

Griffin, W., Andi, Z., O'reilly, S., Ryan, C., 1998. Phanerozoic evolution of the lithosphere beneath the Sino-Korean craton. Mantle Dyn. Plate Interact. East Asia 27, 107–126.

Griffin, W.L., Pearson, N.J., Belousova, E., Jackson, S.E., van Achterbergh, E., O'Reilly, S. Y., Shee, S.R., 2000. The Hf isotope composition of cratonic mantle: LAM-MC-ICPMS analysis of zircon megacrysts in kimberlites. Geochim. Cosmochim. Acta 64, 133–147.
Griffin, W.L., Spetsius, Z.V., Pearson, N.J., O'Reilly, S.Y., 2002. In situ Re-Os analysis of sulfide inclusions in kimberlitic olivine: New constraints on depletion events in the Siberian lithospheric mantle. Geochem. Geophys. Geosyst. 3, 1–25.
Griffin, W.L., Graham, S., O'Reilly, S.Y., Pearson, N.J., 2004. Lithosphere evolution beneath the Kaapvaal Craton: Re–Os systematics of sulfides in mantle-derived peridotites. Chem. Geol. 208, 89–118.
Griffin, W.L., O'Reilly, S.Y., Afonso, J.C., Begg, G.C., 2009. The Composition and Evolution of Lithospheric Mantle: a Re-evaluation and its Tectonic Implications. J. Petrol. 50, 1185–1204.
Griffin, W.L., Nikolic, N., O'Reilly, S.Y., Pearson, N.J., 2012. Coupling, decoupling and metasomatism: evolution of crust–mantle relationships beneath NW Spitsbergen. Lithos 149, 115–135.
Guarnieri, L., Nakamura, E., Piccardo, G.B., Sakaguchi, C., Shimizu, N., Vannucci, R., Zanetti, A., 2012. Petrology, trace element and Sr, Nd, Hf isotope geochemistry of the North Lanzo Peridotite Massif (Western Alps, Italy). J. Petrol. 53, 2259–2306.
Gysi, A.P., Jagoutz, O., Schmidt, M.W., Targuisti, K., 2011. Petrogenesis of pyroxenites and melt infiltrations in the ultramafic complex of Beni Bousera, Northern Morocco. J. Petrol. 52, 1679–1735.
Hammond, J.O.S., Kendall, J.M., Stuart, G.W., Ebinger, C.J., Bastow, I.D., Keir, D., Ayele, A., Belachew, M., Goitom, B., Ogubazghi, G., Wright, T.J., 2013. Mantle upwelling and initiation of rift segmentation beneath the Afar Depression. Geology 41, 635–638.
Hanan, B.B., Blichert-Toft, J., Pyle, D.G., Christie, D.M., 2004. Contrasting origins of the upper mantle revealed by hafnium and lead isotopes from the Southeast Indian Ridge. Nature 432, 91.
Handley, H.K., Turner, S., Macpherson, C.G., Gertisser, R., Davidson, J.P., 2011. Hf–Nd isotope and trace element constraints on subduction inputs at island arcs: limitations of Hf anomalies as sediment input indicators. Earth Planet. Sci. Lett. 304, 212–223.
Hart, S., Hauri, E., Oschmann, L., Whitehead, J., 1992. Mantle plumes and entrainment: isotopic evidence. Science 256, 517–520.
Hawkesworth, C., Mantovani, M., Taylor, P., Palacz, Z., 1986. Evidence from the Parana of South Brazil for a continental contribution to Dupal basalts. Nature 322, 356–359.
Henry, H., Tilhac, R., Griffin, W.L., O'Reilly, S.Y., Satsukawa, T., Kaczmarek, M.-A., Grégoire, M., Ceuleneer, G., 2017. Deformation of mantle pyroxenites provides clues to geodynamic processes in subduction zones: a case study of the Cabo Ortegal complex, Spain. Earth Planet. Sci. Lett. 472, 174–185.
Hirschmann, M.M., Stolper, E.M., 1996. A possible role for garnet pyroxenite in the origin of the "garnet signature" in MORB. Contrib. Mineral. Petrol. 124, 185–208.
Hoernle, K., Tilton, G., Schmincke, H.-U., 1991. SrNdPb isotopic evolution of Gran Canaria: evidence for shallow enriched mantle beneath the Canary Islands. Earth Planet. Sci. Lett. 106, 44–63.
Hofmann, A.W., 1988. Chemical differentiation of the Earth: the relationship between mantle, continental crust, and oceanic crust. Earth Planet. Sci. Lett. 90, 297–314.
Hofmann, A.W., 2014. Sampling mantle heterogeneity through oceanic basalts: Isotopes and trace elements. In: Turekian, K.K. (Ed.), Treatise on Geochemistry, Second edition. Elsevier, Oxford, p. 568.
Hofmann, A.W., Hart, S.R., 1978. An assessment of local and regional isotopic equilibrium in the mantle. Earth Planet. Sci. Lett. 38, 44–62.
Hofmann, A., White, W., 1980. The role of subducted oceanic crust in mantle evolution. Year Book Carnegie Inst. Washington 79, 477–483.
Huang, J.-X., Gréau, Y., Griffin, W.L., O'Reilly, S.Y., Pearson, N.J., 2012. Multi-stage origin of Roberts Victor eclogites: progressive metasomatism and its isotopic effects. Lithos 142–143, 161–181.
Huang, J., Huang, J.-X., Griffin, W.L., Huang, F., 2022. Zn-, Mg- and O-isotope evidence for the origin of mantle eclogites from Roberts Victor kimberlite (Kaapvaal Craton, South Africa). Geology 50, 593–597.
Ionov, D.A., Ashchepkov, I., Jagoutz, E., 2005a. The provenance of fertile off-craton lithospheric mantle: Sr–Nd isotope and chemical composition of garnet and spinel peridotite xenoliths from Vitim, Siberia. Chem. Geol. 217, 41–75.
Ionov, D.A., Blichert-Toft, J., Weis, D., 2005b. Hf isotope compositions and HREE variations in off-craton garnet and spinel peridotite xenoliths from Central Asia. Geochim. Cosmochim. Acta 69, 2399–2418.
Ionov, D.A., Chazot, G., Chauvel, C., Merlet, C., Bodinier, J.-L., 2006. Trace element distribution in peridotite xenoliths from Tok, SE Siberian craton: a record of pervasive, multi-stage metasomatism in shallow refractory mantle. Geochim. Cosmochim. Acta 70, 1231–1260.
Ishikawa, A., Kuritani, T., Makishima, A., Nakamura, E., 2007. Ancient recycled crust beneath the Ontong Java Plateau: isotopic evidence from the garnet clinopyroxenite xenoliths, Malaita, Solomon Islands. Earth Planet. Sci. Lett. 259, 134–148.
Ito, G., Mahoney, J.J., 2005. Flow and melting of a heterogeneous mantle: 1. Method and importance to the geochemistry of ocean island and mid-ocean ridge basalts. Earth Planet. Sci. Lett. 230, 29–46.
Jagoutz, O., Kelemen, P.B., 2015. Role of Arc processes in the formation of continental crust. Annu. Rev. Earth Planet. Sci. 43, 363–404.
Jagoutz, O., Schmidt, M.W., 2013. The composition of the foundered complement to the continental crust and a re-evaluation of fluxes in arcs. Earth Planet. Sci. Lett. 371-372, 177–190.
Janney, P.E., Le Roex, A.P., Carlson, R.W., 2005. Hafnium isotope and trace element constraints on the nature of mantle heterogeneity beneath the Central Southwest Indian Ridge (13°E to 47°E). J. Petrol. 46, 2427–2464.
Janse, A.J.A., 1994. Is Clifford's rule still valid? Affirmative examples from around the world. In: Meyer, H.O.A., Leonardos, O.H. (Eds.), Diamonds: Characterization, Genesis and Exploration. Departement Nacional da Production Mineralia, Brazilia, pp. 215–235.
Johnson, K.T.M., 1998. Experimental determination of partition coefficients for rare earth and high-field-strength elements between clinopyroxene, garnet, and basaltic melt at high pressures. Contrib. Mineral. Petrol. 133, 60–68.
Johnson, C.M., Beard, B.L., 1993. Evidence from hafnium isotopes for ancient sub-oceanic mantle beneath the Rio Grande rift. Nature 362, 441–444.
Jones, R.E., van Keken, P.E., Hauri, E.H., Tucker, J.M., Vervoort, J., Ballentine, C.J., 2019. Origins of the terrestrial Hf-Nd mantle array: evidence from a combined geodynamical-geochemical approach. Earth Planet. Sci. Lett. 518, 26–39.
Kamenetsky, V.S., Maas, R., Sushchevskaya, N.M., Norman, M.D., Cartwright, I., Peyve, A.A., 2001. Remnants of Gondwanan continental lithosphere in oceanic upper mantle: evidence from the South Atlantic Ridge. Geology 29, 243–246.
Koreshkova, M., Downes, H., Nikitina, L., Vladykin, N., Larionov, A., Sergeev, S., 2009. Trace element and age characteristics of zircons in granulite xenoliths from the Udachnaya kimberlite pipe, Siberia. Precambrian Res. 168, 197–212.
Kusky, T.M., Windley, B.F., Wang, L., Wang, Z., Li, X., Zhu, P., 2014. Flat slab subduction, trench suction, and craton destruction: Comparison of the North China, Wyoming, and Brazilian cratons. Tectonophysics 630, 208–221.
Lambart, S., Laporte, D., Provost, A., Schiano, P., 2012. Fate of pyroxenite-derived melts in the peridotitic mantle: thermodynamic and experimental constraints. J. Petrol. 53, 451–476.
Lambart, S., Baker, M.B., Stolper, E.M., 2016. The role of pyroxenite in basalt genesis: Melt-PX, a melting parameterization for mantle pyroxenites between 0.9 and 5 GPa. J. Geophys. Res. Solid Earth 121, 5708–5735.
Lapen, T.J., Medaris, L.G., Johnson, C.M., Beard, B.L., 2005. Archean to Middle Proterozoic evolution of Baltica subcontinental lithosphere: evidence from combined Sm–Nd and Lu–Hf isotope analyses of the Sandvik ultramafic body, Norway. Contrib. Mineral. Petrol. 150, 131–145.
Lazarov, M., Brey, G.P., Weyer, S., 2009. Time steps of depletion and enrichment in the Kaapvaal craton as recorded by subcalcic garnets from Finsch (SA). Earth Planet. Sci. Lett. 279, 1–10.
Lazarov, M., Brey, G.P., Weyer, S., 2012a. Evolution of the south African mantle — a case study of garnet peridotites from the Finsch diamond mine (Kaapvaal craton); part 1: inter-mineral trace element and isotopic equilibrium. Lithos 154, 193–209.
Lazarov, M., Brey, G.P., Weyer, S., 2012b. Evolution of the south African mantle—a case study of garnet peridotites from the Finsch diamond mine (Kaapvaal craton); part 2: multiple depletion and re-enrichment processes. Lithos 154, 210–223.
Le Gall, B., Nonnotte, P., Rolet, J., Benoit, M., Guillou, H., Mousseau-Nonnotte, M., Albaric, J., Deverchère, J., 2008. Rift propagation at craton margin. Tectonophysics 448, 1–19.
Le Roux, V., Bodinier, J.-L., Tommasi, A., Alard, O., Dautria, J.-M., Vauchez, A., Riches, A., 2007. The Lherz spinel lherzolite: refertilized rather than pristine mantle. Earth Planet. Sci. Lett. 259, 599–612.
Le Roux, V., Bodinier, J.L., Alard, O., O'Reilly, S.Y., Griffin, W.L., 2009. Isotopic decoupling during porous melt flow: a case-study in the Lherz peridotite. Earth Planet. Sci. Lett. 279, 76–85.
Lee, C.-T.A., Anderson, D.L., 2015. Continental crust formation at arcs, the arclogite "delamination" cycle, and one origin for fertile melting anomalies in the mantle. Sci. Bull. 60, 1141–1156.
Liu, B., Liang, Y., 2017. The prevalence of kilometer-scale heterogeneity in the source region of MORB upper mantle. Sci. Adv. 3, e1701872.
Liu, C.-Z., Snow, J.E., Hellebrand, E., Brügmann, G., von der Handt, A., Büchl, A., Hofmann, A.W., 2008. Ancient, highly heterogeneous mantle beneath Gakkel ridge, Arctic Ocean. Nature 452, 311–316.
Liu, J., Carlson, R.W., Rudnick, R.L., Walker, R.J., Gao, S., Wu, F.-Y., 2012. Comparative Sr–Nd–Hf–Os–Pb isotope systematics of xenolithic peridotites from Yangyuan, North China Craton: additional evidence for a Paleoproterozoic age. Chem. Geol. 332-333, 1–14.
Liu, C.-Z., Yang, L.-Y., Li, X.-H., Tchouankoue, J.P., 2017a. Age and Sr-Nd-Hf isotopes of the sub-continental lithospheric mantle beneath the Cameroon Volcanic Line: constraints from the Nyos mantle xenoliths. Chem. Geol. 455, 84–97.
Liu, C.-Z., Zhang, C., Liu, Z.-C., Sun, J., Chu, Z.-Y., Qiu, Z.-L., Wu, F.-Y., 2017b. Formation age and metasomatism of the sub-continental lithospheric mantle beneath Southeast China: Sr-Nd-Hf-Os isotopes of Mingxi mantle xenoliths. J. Asian Earth Sci. 145, 591–604.
Liu, J., Pearson, D.G., Shu, Q., Sigurdsson, H., Thomassot, E., Alard, O., 2019. Dating post-Archean lithospheric mantle: Insights from Re-Os and Lu-Hf isotopic systematics of the Cameroon Volcanic Line peridotites. Geochim. Cosmochim. Acta 278, 177–198.
Liu, T., Wu, F.-Y., Liu, C.-Z., Eyuboglu, Y., Zhu, D.-C., Zhang, C., Ji, W.-B., Xu, Y., Zhang, Z.-Y., 2020. Testing oceanic crust–mantle decoupling by Sr–Nd–Hf–Os isotopes of Neo-Tethyan ophiolites. Lithos 376–377.
Liu, C.-Z., Dick, H.J.B., Mitchell, R.N., Wei, W., Zhang, Z.-Y., Hofmann, A.W., Yang, J.-F., Li, Y., 2022. Archean cratonic mantle recycled at a mid-ocean ridge. Science. Advances 8 eabn6749.
van de Löcht, J., Hoffmann, J.E., Rosing, M.T., Sprung, P., Münker, C., 2020. Preservation of Eoarchean mantle processes in ~3.8 Ga peridotite enclaves in the Itsaq Gneiss complex, southern West Greenland. Geochim. Cosmochim. Acta 280, 1–25.
Lu, J., Griffin, W.L., Tilhac, R., Xiong, Q., Zheng, J., O'Reilly, S.Y., 2018. Tracking deep lithospheric events with garnet-Websterite Xenoliths from Southeastern Australia. J. Petrol. 59, 901–930.
Lu, J., Tilhac, R., Griffin, W.L., Zheng, J., Xiong, Q., Oliveira, B., O'Reilly, S.Y., 2020. Lithospheric memory of subduction in mantle pyroxenite xenoliths from rift-related basalts. Earth Planet. Sci. Lett. 544.

Lustrino, M., 2005. How the delamination and detachment of lower crust can influence basaltic magmatism. Earth Sci. Rev. 72, 21–38.
Mahoney, J., Natland, J., White, W., Poreda, R., Bloomer, S., Fisher, R., Baxter, A., 1989. Isotopic and geochemical provinces of the western Indian Ocean spreading centers. J. Geophys. Res. Solid Earth 94, 4033–4052.
Mahoney, J., Le Roex, A., Peng, Z., Fisher, R., Natland, J., 1992. Southwestern limits of Indian Ocean Ridge mantle and the origin of low 206Pb/204Pb mid-ocean ridge basalt: isotope systematics of the central Southwest Indian Ridge (17–50 E). J. Geophys. Res. Solid Earth 97, 19771–19790.
Malaviarachchi, S.P., Makishima, A., Tanimoto, M., Kuritani, T., Nakamura, E., 2008. Highly unradiogenic lead isotope ratios from the Horoman peridotite in Japan. Nat. Geosci. 1, 859–863.
Malaviarachchi, S.P.K., Makishima, A., Nakamura, E., 2010. Melt–peridotite reactions and fluid metasomatism in the Upper Mantle, revealed from the geochemistry of peridotite and gabbro from the Horoman Peridotite Massif, Japan. J. Petrol. 51, 1417–1445.
Mallick, S., Dick, H.J.B., Sachi-Kocher, A., Salters, V.J.M., 2014. Isotope and trace element insights into heterogeneity of subridge mantle. Geochem. Geophys. Geosyst. 15, 2438–2453.
Mallick, S., Standish, J.J., Bizimis, M., 2015. Constraints on the mantle mineralogy of an ultra-slow ridge: Hafnium isotopes in abyssal peridotites and basalts from the 9–25°E Southwest Indian Ridge. Earth Planet. Sci. Lett. 410, 42–53.
McDonough, W.F., Sun, S.S., 1995. The composition of the Earth. Chem. Geol. 120, 223–253.
McKenzie, D., O'nions, R., 1983. Mantle reservoirs and ocean island basalts. Nature 301, 229–231.
Medaris, L.G., Beard, B.L., Johnson, C.M., Valley, J.W., Spicuzza, M.J., Jelínek, E., Mísâr, Z., 1995. Garnet pyroxenite and eclogite in the Bohemian Massif: geochemical evidence for Variscan recycling of subducted lithosphere. Geol. Rundsch. 84, 489–505.
Meng, F., Xu, W., Xu, Q., Guo, J., Zhang, Y., 2019. Decoupling of Lu-Hf and Sm-Nd Isotopic system in deep-seated xenoliths from the Xuzhou-Suzhou Area, China: differences in element mobility during metamorphism. J. Earth Sci. 30, 1266–1279.
Milner, S.C., le Roex, A.P., 1996. Isotope characteristics of the Okenyenya igneous complex, northwestern Namibia: constraints on the composition of the early Tristan plume and the origin of the EM 1 mantle component. Earth Planet. Sci. Lett. 141, 277–291.
Montanini, A., Tribuzio, R., 2015. Evolution of recycled crust within the mantle: Constraints from the garnet pyroxenites of the External Ligurian ophiolites (northern Apennines, Italy). Geology 43, 911–914.
Montanini, A., Tribuzio, R., Anczkiewicz, R., 2006. Exhumation history of a garnet pyroxenite-bearing mantle section from a continent–ocean transition (Northern Apennine Ophiolites, Italy). J. Petrol. 47, 1943–1971.
Montanini, A., Tribuzio, R., Thirlwall, M., 2012. Garnet clinopyroxenite layers from the mantle sequences of the Northern Apennine ophiolites (Italy): evidence for recycling of crustal material. Earth Planet. Sci. Lett. 351–352, 171–181.
Niu, Y., Wilson, M., Humphreys, E.R., O'Hara, M.J., 2011. The origin of intra-plate Ocean Island Basalts (OIB): the lid effect and its geodynamic implications. J. Petrol. 52, 1443–1468.
Oliveira, B., Afonso, J.C., Tilhac, R., 2020. A disequilibrium reactive transport model for mantle magmatism. J. Petrol. 61.
O'Reilly, S.Y., Zhang, M., Griffin, W.L., Begg, G., Hronsky, J., 2009. Ultradeep continental roots and their oceanic remnants: a solution to the geochemical "mantle reservoir" problem? Lithos 112, 1043–1054.
Park, K., Choi, S.H., Cho, M., Lee, D.-C., 2017. Evolution of the lithospheric mantle beneath Mt. Baekdu (Changbaishan): constraints from geochemical and Sr–Nd–Hf isotopic studies on peridotite xenoliths in trachybasalt. Lithos 286, 330–344.
Patchett, P.J., 1983. Hafnium isotope results from mid-ocean ridges and Kerguelen. Lithos 16, 47–51.
Patchett, P.J., Tatsumoto, M., 1980a. Hafnium isotope variations in oceanic basalts. Geophys. Res. Lett. 7, 1077–1080.
Patchett, P.J., Tatsumoto, M., 1980b. Lu–Hf total-rock isochron for the eucrite meteorites. Nature 288, 571.
Patchett, P.J., White, W.M., Feldmann, H., Kielinczuk, S., Hofmann, A.W., 1984. Hafnium/rare earth element fractionation in the sedimentary system and crustal recycling into the Earth's mantle. Earth Planet. Sci. Lett. 69, 365–378.
Pearce, J.A., Kempton, P.D., Nowell, G.M., Noble, S.R., 1999. Hf-Nd element and isotope perspective on the nature and provenance of mantle and subduction components in Western Pacific Arc-Basin Systems. J. Petrol. 40, 1579–1611.
Pearson, D.G., Nowell, G.M., 2004. Re–Os and Lu–Hf isotope constraints on the origin and age of pyroxenites from the beni bousera peridotite massif: implications for mixed peridotite–pyroxenite mantle sources. J. Petrol. 45, 439–455.
Pearson, D., Davies, G., Nixon, P., 1995. Orogenic ultramafic rocks of UHP (diamond facies) origin. Ultrahigh Pressure Metamorphism 456–510.
Pearson, D.G., Canil, D., Shirey, S.B., 2014. Mantle samples included in volcanic rocks: xenoliths and diamonds. In: Turekian, K.K. (Ed.), Treatise on Geochemistry, Second edition, pp. 169–253.
Petit, C., Ebinger, C., 2000. Flexure and mechanical behavior of cratonic lithosphere: gravity models of the East African and Baikal rifts. J. Geophys. Res. Solid Earth 105, 19151–19162.
Rampone, E., Hofmann, A.W., 2012. A global overview of isotopic heterogeneities in the oceanic mantle. Lithos 148, 247–261.
Rampone, E., Sanfilippo, A., 2021. The heterogeneous tethyan oceanic lithosphere of the alpine ophiolites. Elements 17, 23–28.
le Roux, P.J., le Roex, A.P., Schilling, J.G., Shimizu, N., Perkins, W.W., Pearce, N.J.G., 2002. Mantle heterogeneity beneath the southern Mid-Atlantic Ridge: trace element evidence for contamination of ambient asthenospheric mantle. Earth Planet. Sci. Lett. 203, 479–498.
Saal, A.E., Hart, S.R., Shimizu, N., Hauri, E.H., Layne, G.D., 1998. Pb isotopic variability in melt inclusions from Oceanic Island Basalts, Polynesia. Science 282, 1481–1484.
Salters, V.J.M., 1994. 176Hf/177Hf determination in small samples by a high-temperature SIMS technique. Anal. Chem. 66, 4186–4189.
Salters, V.J.M., 1996. The generation of mid-ocean ridge basalts from the Hf and Nd isotope perspective. Earth Planet. Sci. Lett. 141, 109–123.
Salters, V.J.M., Dick, H.J.B., 2002. Mineralogy of the mid-ocean-ridge basalt source from neodymium isotopic composition of abyssal peridotites. Nature 418, 68–72.
Salters, V.J.M., Hart, S.R., 1989. The hafnium paradox and the role of garnet in the source of mid-ocean-ridge basalts. Nature 342, 420.
Salters, V.J.M., Hart, S.R., 1991. The mantle sources of ocean ridges, islands and arcs: the Hf-isotope connection. Earth Planet. Sci. Lett. 104, 364–380.
Salters, V.J.M., Shimizu, N., 1988. World-wide occurrence of HFSE-depleted mantle. Geochim. Cosmochim. Acta 52, 2177–2182.
Salters, V.J.M., Stracke, A., 2004. Composition of the depleted mantle. Geochem. Geophys. Geosyst. 5 n/a-n/a.
Salters, V.J.M., White, W.M., 1998. Hf isotope constraints on mantle evolution. Chem. Geol. 145, 447–460.
Salters, V.J.M., Zindler, A., 1995. Extreme 176Hf/177Hf in the sub-oceanic mantle. Earth Planet. Sci. Lett. 129, 13–30.
Salters, V.J.M., Mallick, S., Hart, S.R., Langmuir, C.E., Stracke, A., 2011. Domains of depleted mantle: new evidence from hafnium and neodymium isotopes. Geochem. Geophys. Geosyst. 12.
Sanfilippo, A., Salters, V., Tribuzio, R., Zanetti, A., 2019. Role of ancient, ultra-depleted mantle in Mid-Ocean-Ridge magmatism. Earth Planet. Sci. Lett. 511, 89–98.
Sanfilippo, A., Salters, V.J.M., Sokolov, S.Y., Peyve, A.A., Stracke, A., 2021. Ancient refractory asthenosphere revealed by mantle re-melting at the Arctic Mid Atlantic Ridge. Earth Planet. Sci. Lett. 566.
Sanfilippo, A., Borghini, G., Guarnieri, L., Nakamura, E., Piccardo, G.B., Vannucci, R., Zanetti, A., 2022. A 400 Ma-long Nd-Hf isotopic evolution of melt-modified garnet-pyroxenites in an ancient subcontinental lithosphere (Lanzo North ophiolite, Western Alps). Chem. Geol. 588.
Santos, J.F., Schärer, U., Gil Ibarguchi, J.I., Girardeau, J., 2002. Genesis of pyroxenite-rich peridotite at Cabo Ortegal (NW Spain): geochemical and Pb–Sr–Nd isotope data. J. Petrol. 43, 17–43.
Santos, R.V., Ganade, C.E., Lacasse, C.M., Costa, I.S.L., Pessanha, I., Frazão, E.P., Dantas, E.L., Cavalcante, J.A., 2019. Dating Gondwanan continental crust at the Rio Grande rise, South Atlantic. Terra Nova 31, 424–429.
Scherer, E.E., Cameron, K.L., Blichert-Toft, J., 2000. Lu–Hf garnet geochronology: closure temperature relative to the Sm–Nd system and the effects of trace mineral inclusions. Geochim. Cosmochim. Acta 64, 3413–3432.
Scherer, E., Münker, C., Mezger, K., 2001. Calibration of the lutetium-hafnium clock. Science 293, 683–687.
Schmidberger, S.S., Simonetti, A., Francis, D., 2001. Sr-Nd-Pb isotope systematics of mantle xenoliths from Somerset Island kimberlites: Evidence for lithosphere stratification beneath Arctic Canada. Geochim. Cosmochim. Acta. 65, 4243–4255.
Schmidberger, S.S., Simonetti, A., Francis, D., Gariépy, C., 2002. Probing Archean lithosphere using the Lu–Hf isotope systematics of peridotite xenoliths from Somerset Island kimberlites, Canada. Earth Planet. Sci. Lett. 197, 245–259.
Schmitz, M.D., Bowring, S.A., de Wit, M.J., Gartz, V., 2004. Subduction and terrane collision stabilize the western Kaapvaal craton tectosphere 2.9 billion years ago. Earth Planet. Sci. Lett. 222, 363–376.
Sdrolias, M., Müller, R.D., 2006. Controls on back-arc basin formation. Geochem. Geophys. Geosyst. 7.
Shaw, J.E., Baker, J.A., Kent, A.J.R., Ibrahim, K.M., Menzies, M.A., 2007. The geochemistry of the Arabian lithospheric mantle – a source for intraplate volcanism? J. Petrol. 48, 1495–1512.
Shen, Y., Forsyth, D.W., 1995. Geochemical constraints on initial and final depths of melting beneath mid-ocean ridges. J. Geophys. Res. Solid Earth 100, 2211–2237.
Shirey, S.B., Bender, J.F., Langmuir, C.H., 1987. Three-component isotopic heterogeneity near the Oceanographer transform, Mid-Atlantic Ridge. Nature 325, 217–223.
Shu, Q., Brey, G.P., 2015. Ancient mantle metasomatism recorded in subcalcic garnet xenocrysts: Temporal links between mantle metasomatism, diamond growth and crustal tectonomagmatism. Earth Planet. Sci. Lett. 418, 27–39.
Shu, Q., Brey, G.P., Gerdes, A., Hoefer, H.E., 2013. Geochronological and geochemical constraints on the formation and evolution of the mantle underneath the Kaapvaal craton: Lu–Hf and Sm–Nd systematics of subcalcic garnets from highly depleted peridotites. Geochim. Cosmochim. Acta 113, 1–20.
Shu, Q., Brey, G.P., Gerdes, A., Hoefer, H.E., 2014. Mantle eclogites and garnet pyroxenites – the meaning of two-point isochrons, Sm–Nd and Lu–Hf closure temperatures and the cooling of the subcratonic mantle. Earth Planet. Sci. Lett. 389, 143–154.
Shu, Q., Brey, G.P., Pearson, D.G., Liu, J., Gibson, S.A., Becker, H., 2019. The evolution of the Kaapvaal craton: a multi-isotopic perspective from lithospheric peridotites from Finsch diamond mine. Precambrian Res. 331.
Siegrist, M., Yogodzinski, G., Bizimis, M., Fournelle, J., Churikova, T., Dektor, C., Mobley, R., 2019. Fragments of metasomatized forearc: origin and implications of mafic and ultramafic xenoliths from Kharchinsky Volcano, Kamchatka. Geochem. Geophys. Geosyst. 20, 4426–4456.
Simon, N.S.C., Carlson, R.W., Pearson, D.G., Davies, G.R., 2007. The origin and evolution of the Kaapvaal Cratonic lithospheric mantle. J. Petrol. 48, 589–625.
Snow, J.E., 1993. The Isotope Geochemistry of Abyssal Peridotites and Related Rocks. Woods Hole Oceanographic Institution - Dept Of Applied Ocean Physics And Engineering.

Snow, J.E., Hart, S.R., Dick, H.J.B., 1994. Nd and Sr isotope evidence linking mid-ocean-ridge basalts and abyssal peridotites. Nature 371, 57–60.
Staudigel, H., Park, K.H., Pringle, M., Rubenstone, J.L., Smith, W.H.F., Zindler, A., 1991. The longevity of the South Pacific isotopic and thermal anomaly. Earth Planet. Sci. Lett. 102, 24–44.
Storey, M., Saunders, A.D., Tarney, J., Gibson, I.L., Norry, M.J., Thirlwall, M.F., Leat, P., Thompson, R.N., Menzies, M.A., 1989. Contamination of Indian Ocean asthenosphere by the Kerguelen–Heard mantle plume. Nature 338, 574.
Stracke, A., 2012. Earth's heterogeneous mantle: a product of convection-driven interaction between crust and mantle. Chem. Geol. 330-331, 274–299.
Stracke, A., 2021. A process-oriented approach to mantle geochemistry. Chem. Geol. 579.
Stracke, A., Bizimis, M., Salters, V.J.M., 2003. Recycling oceanic crust: quantitative constraints. Geochem. Geophys. Geosyst. 4.
Stracke, A., Hofmann, A.W., Hart, S.R., 2005. FOZO, HIMU, and the rest of the mantle zoo. Geochem. Geophys. Geosyst. 6.
Stracke, A., Snow, J.E., Hellebrand, E., von der Handt, A., Bourdon, B., Birbaum, K., Günther, D., 2011. Abyssal peridotite Hf isotopes identify extreme mantle depletion. Earth Planet. Sci. Lett. 308, 359–368.
Stracke, A., Genske, F., Berndt, J., Koornneef, J.M., 2019. Ubiquitous ultra-depleted domains in Earth's mantle. Nat. Geosci. 12, 851–855.
Sun, P., Guo, P., Niu, Y., 2021. Eastern China continental lithosphere thinning is a consequence of paleo-Pacific plate subduction: a review and new perspectives. Earth Sci. Rev. 218.
Svojtka, M., Ackerman, L., Medaris, L.G., Hegner, E., Valley, J.W., Hirajima, T., Jelínek, E., Hrstka, T., 2016. Petrological, geochemical and Sr–Nd–O isotopic constraints on the origin of garnet and spinel pyroxenites from the Moldanubian Zone of the Bohemian Massif. J. Petrol. 57, 897–920.
Takazawa, E., 1996. Geodynamic Evolution of the Horoman Peridotite, Japan: Geochemical Study of Asthenospheric and Lithospheric Processes. Massachusetts Institute of Technology, p. 562.
Takazawa, E., Frey, F.A., Shimizu, N., Yoshikawa, M., Nakamura, E., 1995. Geodynamic evolution of the Horoman peridotite, Hokkaido, Japan based on geochemical studies of a 140m stratigraphic section. In: 2nd International Workshop on Orogenic Lherzolites and Mantle Processes, Granada, Spain, pp. 68–69.
Tang, Y.-J., Zhang, H.-F., Ying, J.-F., Su, B.-X., 2013. Widespread refertilization of cratonic and circum-cratonic lithospheric mantle. Earth Sci. Rev. 118, 45–68.
Tang, M., Rudnick, R.L., McDonough, W.F., Gaschnig, R.M., Huang, Y., 2015. Europium anomalies constrain the mass of recycled lower continental crust. Geology 43, 703–706.
Tatsumi, Y., 2000. Continental crust formation by crustal delamination in subduction zones and complementary accumulation of the enriched mantle I component in the mantle. Geochem. Geophys. Geosyst. 1.
Teklay, M., Scherer, E.E., Mezger, K., Danyushevsky, L., 2010. Geochemical characteristics and Sr–Nd–Hf isotope compositions of mantle xenoliths and host basalts from Assab, Eritrea: implications for the composition and thermal structure of the lithosphere beneath the Afar Depression. Contrib. Mineral. Petrol. 159, 731–751.
Tilhac, R., 2017. Petrology and Geochemistry of Pyroxenites from the Cabo Ortegal Complex, Spain. Macquarie University, p. 230.
Tilhac, R., Ceuleneer, G., Griffin, W.L., O'Reilly, S.Y., Pearson, N.J., Benoit, M., Henry, H., Girardeau, J., Grégoire, M., 2016. Primitive arc magmatism and delamination: petrology and geochemistry of pyroxenites from the Cabo Ortegal complex, Spain. J. Petrol. 57, 1921–1954.
Tilhac, R., Grégoire, M., O'Reilly, S.Y., Griffin, W.L., Henry, H., Ceuleneer, G., 2017. Sources and timing of pyroxenite formation in the sub-arc mantle: case study of the Cabo Ortegal complex, Spain. Earth Planet. Sci. Lett. 474, 490–502.
Tilhac, R., Oliveira, B., Griffin, W.L., O'Reilly, S.Y., Schaefer, B.F., Alard, O., Ceuleneer, G., Afonso, J.C., Grégoire, M., 2020. Reworking of old continental lithosphere: Unradiogenic Os and decoupled Hf Nd isotopes in sub-arc mantle pyroxenites. Lithos 354–355.
Tilhac, R., Morishita, T., Hanaue, N., Tamura, A., Guotana, J.M., 2021. Systematic LREE enrichment of mantle harzburgites: the petrogenesis of San Carlos xenoliths revisited. Lithos 396–397.
Tretiakova, I.G., Belousova, E.A., Malkovets, V.G., Griffin, W.L., Piazolo, S., Pearson, N. J., O'Reilly, S.Y., Nishido, H., 2017. Recurrent magmatic activity on a lithosphere-scale structure: crystallization and deformation in kimberlitic zircons. Gondwana Res. 42, 126–132.
Urann, B.M., Dick, H.J.B., Parnell-Turner, R., Casey, J.F., 2020. Recycled arc mantle recovered from the Mid-Atlantic Ridge. Nat. Commun. 11, 3887.
Van Kranendonk, M.J., Hugh Smithies, R., Hickman, A.H., Champion, D.C., 2007. Review: secular tectonic evolution of Archean continental crust: interplay between horizontal and vertical processes in the formation of the Pilbara Craton, Australia. Terra Nova 19, 1–38.
Van Orman, J.A., Grove, T.L., Shimizu, N., 2001. Rare earth element diffusion in diopside: influence of temperature, pressure, and ionic radius, and an elastic model for diffusion in silicates. Contrib. Mineral. Petrol. 141, 687–703.
Van Orman, J.A., Grove, T.L., Shimizu, N., 2002. Diffusive fractionation of trace elements during production and transport of melt in Earth's upper mantle. Earth Planet. Sci. Lett. 198, 93–112.
Varas-Reus, M.I., Garrido, C.J., Marchesi, C., Bosch, D., Hidas, K., 2018. Genesis of ultra-high pressure garnet pyroxenites in orogenic peridotites and its bearing on the compositional heterogeneity of the Earth's mantle. Geochim. Cosmochim. Acta 232, 303–328.
Vervoort, J., 2014. Lu-Hf dating: the Lu-Hf isotope system. In: Encyclopedia of Scientific Dating Methods, pp. 1–20.
Vervoort, J.D., Blichert-Toft, J., 1999. Evolution of the depleted mantle: Hf isotope evidence from juvenile rocks through time. Geochim. Cosmochim. Acta 63, 533–556.
Vervoort, J.D., Patchett, P.J., Blichert-Toft, J., Albarède, F., 1999. Relationships between Lu–Hf and Sm–Nd isotopic systems in the global sedimentary system. Earth Planet. Sci. Lett. 168, 79–99.
Vervoort, J.D., Patchett, P.J., Albarède, F., Blichert-Toft, J., Rudnick, R., Downes, H., 2000. Hf–Nd isotopic evolution of the lower crust. Earth Planet. Sci. Lett. 181, 115–129.
Vervoort, J.D., Plank, T., Prytulak, J., 2011. The Hf–Nd isotopic composition of marine sediments. Geochim. Cosmochim. Acta 75, 5903–5926.
Waight, T.E., Troll, V.R., Gamble, J.A., Price, R.C., Chadwick, J.P., 2017. Hf isotope evidence for variable slab input and crustal addition in basalts and andesites of the Taupo Volcanic Zone, New Zealand. Lithos 284-285, 222–236.
Warren, J.M., Shimizu, N., Sakaguchi, C., Dick, H.J.B., Nakamura, E., 2009. An assessment of upper mantle heterogeneity based on abyssal peridotite isotopic compositions. J. Geophys. Res. Solid Earth 114 n/a-n/a.
White, W.M., Patchett, J., 1984. HfNdSr isotopes and incompatible element abundances in island arcs: implications for magma origins and crust-mantle evolution. Earth Planet. Sci. Lett. 67, 167–185.
White, W.M., Patchett, J., BenOthman, D., 1986. Hf isotope ratios of marine sediments and Mn nodules: evidence for a mantle source of Hf in seawater. Earth Planet. Sci. Lett. 79, 46–54.
Widom, E., Hoernle, K.A., Shirey, S., Schmincke, H.-U., 1999. Os isotope systematics in the Canary Islands and Madeira: lithospheric contamination and mantle plume signatures. J. Petrol. 40, 279–296.
Willbold, M., Stracke, A., 2010. Formation of enriched mantle components by recycling of upper and lower continental crust. Chem. Geol. 276, 188–197.
Wittig, N., Baker, J.A., Downes, H., 2006. Dating the mantle roots of young continental crust. Geology 34.
Wittig, N., Baker, J.A., Downes, H., 2007. U–Th–Pb and Lu–Hf isotopic constraints on the evolution of sub-continental lithospheric mantle, French Massif Central. Geochim. Cosmochim. Acta 71, 1290–1311.
Wittig, N., Pearson, D.G., Duggen, S., Baker, J.A., Hoernle, K., 2010. Tracing the metasomatic and magmatic evolution of continental mantle roots with Sr, Nd, Hf and and Pb isotopes: a case study of Middle Atlas (Morocco) peridotite xenoliths. Geochim. Cosmochim. Acta 74, 1417–1435.
Workman, R.K., Hart, S.R., 2005. Major and trace element composition of the depleted MORB mantle (DMM). Earth Planet. Sci. Lett. 231, 53–72.
Wu, F.-Y., Walker, R.J., Yang, Y.-H., Yuan, H.-L., Yang, J.-H., 2006. The chemical-temporal evolution of lithospheric mantle underlying the North China Craton. Geochim. Cosmochim. Acta 70, 5013–5034.
Wu, F.-Y., Yang, J.-H., Xu, Y.-G., Wilde, S.A., Walker, R.J., 2019. Destruction of the North China Craton in the Mesozoic. Annu. Rev. Earth Planet. Sci. 47, 173–195.
Xiong, Q., Zheng, J.-P., Griffin, W.L., O'Reilly, S.Y., Pearson, N.J., 2014. Pyroxenite dykes in orogenic peridotite from North Qaidam (NE Tibet, China) track metasomatism and segregation in the Mantle Wedge. J. Petrol. 55, 2347–2376.
Xu, Y., Liu, C.-Z., Lin, W., 2021. Melt extraction and reaction in the forearc mantle: constraints from trace elements and isotope geochemistry of ultra-refractory peridotites of the New Caledonia Peridotite Nappe. Lithos 380–381.
Yang, J.-H., Wu, F.-Y., Wilde, S.A., Belousova, E., Griffin, W.L., 2008. Mesozoic decratonization of the North China block. Geology 36, 467–470.
Yang, J.-H., O'Reilly, S., Walker, R.J., Griffin, W., Wu, F.-Y., Zhang, M., Pearson, N., 2010. Diachronous decratonization of the Sino-Korean craton: geochemistry of mantle xenoliths from North Korea. Geology 38, 799–802.
Yang, J.-H., Zhang, M., Wu, F.-Y., 2018. Mesozoic decratonization of the North China Craton by lithospheric delamination: evidence from Sr-Nd-Hf-Os isotopes of mantle xenoliths of Cenozoic alkaline basalts in Yangyuan, Hebei Province, China. J. Asian Earth Sci. 160, 396–407.
Yogodzinski, G.M., Vervoort, J.D., Brown, S.T., Gerseny, M., 2010. Subduction controls of Hf and Nd isotopes in lavas of the Aleutian island arc. Earth Planet. Sci. Lett. 300, 226–238.
Yoshikawa, M., Nakamura, E., 2000. Geochemical evolution of the Horoman peridotite complex: Implications for melt extraction, metasomatism, and compositional layering in the mantle. J. Geophys. Res. Solid Earth 105, 2879–2901.
Yu, S.-Y., Xu, Y.-G., Huang, X.-L., Ma, J.-L., Ge, W.-C., Zhang, H.-H., Qin, X.-F., 2009. Hf–Nd isotopic decoupling in continental mantle lithosphere beneath Northeast China: effects of pervasive mantle metasomatism. J. Asian Earth Sci. 35, 554–570.
Zangana, N.A., Downes, H., Thirlwall, M.F., Hegner, E., 1997. Relationship between deformation, equilibration temperatures, REE and radiogenic isotopes in mantle xenoliths (Ray Pic, Massif Central, France): an example of plume-lithosphere interaction? Contrib. Mineral. Petrol. 127, 187–203.
Zhang, M., Yang, J.-H., Sun, J.-F., Wu, F.-Y., Zhang, M., 2012. Juvenile subcontinental lithospheric mantle beneath the eastern part of the Central Asian Orogenic Belt. Chem. Geol. 328, 109–122.
Zhang, C., Liu, C.-Z., Liu, T., Wu, F.-Y., 2020. Evolution of mantle peridotites from the Luobusa ophiolite in the Tibetan Plateau: Sr-Nd-Hf-Os isotope constraints. Lithos 362–363.
Zhao, G., Cawood, P.A., Wilde, S.A., Sun, M., 2002. Review of global 2.1–1.8 Ga orogens: implications for a pre-Rodinia supercontinent. Earth Sci. Rev. 59, 125–162.
Zhao, W., Sun, Y., Balsam, W., Lu, H., Liu, L., Chen, J., Ji, J., 2014. Hf-Nd isotopic variability in mineral dust from Chinese and Mongolian deserts: implications for sources and dispersal. Sci. Rep. 4, 5837.

Zhao, G., Sun, M., Wilde, S.A., Li, S., 2004. A Paleo-Mesoproterozoic supercontinent: assembly, growth and breakup. Earth Sci. Rev. 67, 91–123.
Zhao, X., Wang, H., Li, Z., Evans, N.J., Ying, J., Yang, Y., Zhang, H., 2021. Nature and evolution of lithospheric mantle beneath the western North China Craton: Constraints from peridotite and pyroxenite xenoliths in the Sanyitang basalts. Lithos 384–385.
Zindler, A., Hart, S., 1986. Chemical Geodynamics. Annu. Rev. Earth Planet. Sci. 14, 493–571.